Journal of Materials Research and Technology 30 (2024) 5605–5621

Contents lists available at ScienceDirect

Journal of Materials Research and Technology

journal homepage: www.elsevier.com/locate/jmrt

Stainless steels as a solution for corrosion and erosion problems involving grains in agribusiness sector applications

Vitor Pagani de Souza [a,b], Wilian da Silva Labiapari [b], Vanessa de Freitas Cunha Lins [a,*]

[a] Engineering School, Universidade Federal de Minas Gerais, Belo Horizonte, 31270901, Brazil
[b] Aperam South America, Timóteo, 35180018, Brazil

ARTICLE INFO

Handling editor: M Meyers

Keywords:
Erosion-corrosion
Ferritic stainless steel
High-strength carbon steel
Chlorides
Corn particles
Austenitic stainless steel

ABSTRACT

Agricultural activities such as grain processing play a crucial role in Brazil's economy, contributing significantly to its gross domestic product (27.4% in 2021). The use of carbon steel equipment leads to considerable environmental and economic losses in agribusiness due to corrosion. This study explores the erosion-corrosion behavior of a dual-phase 11Cr and an 18Cr8Ni stainless steel (SS), compared to a mild (ASTM A36) and a high-strength carbon (AHSS) steel under conditions close to the agribusiness reality. The impact of corn particles as erosive component associated to pure water and chloride-containing environments was studied using a fog chamber, a topic until now unexplored in the literature. The methodology adopted is novel and explores the erosion-corrosion synergy in cumulative steps, aiming to shed light on the mechanisms of corrosion and wear that affect the materials in the agribusiness industry. The findings reveal that corn particles, despite their soft nature, can easily remove non-adherent corrosion products from the steel surface. In the deionized water medium, the impact of the soft particles can also shift the corrosion pattern of advanced high-strength steels from general corrosion to localized pitting damage reduzing the corrosion rates. The carbon and 11Cr steels showed the highest corrosion rates under the pure corrosion condition in both media. The erosion-corrosion process considerably reduced the corrosion rate, mainly in the deionized water medium for the carbon steels. An exception to this behavior was 18Cr8Ni steel, whose corrosion rates, however, were the lowest among the materials. Low-chromium stainless steel emerges as a cost-effective solution to erosion-corrosion challenges in the agribusiness segment.

1. Introduction

Comprising a set of economic activities connected to the agricultural sector, agribusiness serves as the driving force for Brazil progress, accounting for a quarter of the country's GDP [1,2]. However, with the advancement of technology and the demand for increase productivity it has become a high-energy consumption industry. According to data from the Food and Agriculture Organization – FAO of the United Nations [3] agriculture is responsible for 21% of global pollutant gas emissions, second only to the energy sector (47%), which includes the steel production industry (10.5%) [4]. In addition to the pressure imposed by operational costs, such as the rising of agricultural inputs [1,2], recurring expenses for repairs and replacements of carbon steel equipment due to corrosion do not affect only the competitiveness of the sector. Global economic losses as a result of this phenomenon have been known for many decades [5] but little attention is still given to its environmental impact. Despite the relevance of direct losses (3.4% of world GDP in 2016 [5]), indirect losses extend beyond the economic sphere and are more concerning and challenging to quantify [6]. Iannuzzi and Frankel [4] correlated the impact of steel corrosion on the emission of pollutant gases such as carbon dioxide (CO_2). The global steel production was responsible for emitting nearly 3.8 Gt of CO_2 in 2021, of which up to 1200 Mt can be associated with the production directed to replace the amount destroyed by corrosion. In this context, green steels such as stainless steel, produced from renewable energy sources and carbon-neutral footprint [7], in addition to being more durable solutions, can contribute to reducing the environmental impacts resulting from steel corrosion [6].

Despite having a low corrosion and wear resistance, conventional carbon steels are the primary material used in agricultural structures and equipment [8,9]. Advanced high-strength carbon steels (AHSS) are also used, but only when high wear resistance is required [10].

* Corresponding author.
E-mail addresses: vlins@deq.ufmg.br, vfclins@gmail.com (V. de Freitas Cunha Lins).

https://doi.org/10.1016/j.jmrt.2024.04.203
Received 5 March 2024; Received in revised form 17 April 2024; Accepted 23 April 2024
Available online 26 April 2024

However, the tribological performance of these steels is inadequate in some engineering applications that involve corrosive environments [11] such as agribusiness. The presence of water is a non-negligible factor in agricultural applications [9], whether due to grain moisture, process temperature or simple atmospheric exposure. Furthermore, contaminants such as chlorides from fertilizers can also be dragged by the grains to the steel surface and increase corrosiveness [12,13]. The erosion-corrosion of carbon steels in aqueous environments is significantly influenced by the chemical composition of the solution involved [8]. Thus, numerous works in the literature aim to enhance this understanding, especially in media containing chlorides [8,14–16].

Stainless steels are still predominantly used in applications where corrosion resistance is a dominant requirement, for aesthetic and functional aspects, and are rarely used when the primary objective is wear resistance [9]. Given their relevance, wear mechanisms such as erosion already been systematically studied in synergy with corrosion in neighboring sectors such as mining [16–21]. There are some specific conditions where grain processing shows more aggressive wear components to the materials, as reported by Camacho et al. [22] regarding the thickness premature reduction of a classifying chute made of aluminum operating with rice grains while with husk, which is very abrasive. However, in the case of softer solid particles such as grains (e.g., corn, soybean, among others), the mechanical component in agribusiness tends to be less aggressive than steel when compared to those observed on mining (e.g., silica, ores, among others). Karafyllias et al. [23] reported results where an AISI 316 (18Cr8Ni2Mo) steel exhibited identical rates of pure corrosion and erosion-corrosion in a saline environment (pH between 7 and 3) with the presence of silica particles. The passive film formed was not damaged by the milder erosive conditions, and the low hardness and wear resistance of AISI 316 steel made the corrosion resistance more important. The literature presents several studies regarding erosion-corrosion of conventional austenitic steels such as AISI 304 and AISI 316 [18,19,21,24] and also high-chromium alloys [23,25], which are very expensive materials. Comparative studies between stainless and carbon steels are also common [26–28] but a gap is evident for studies directed towards agribusiness sector. Furthermore, a small number of studies focused more commercially attractive steels such as low-chromium grades like AISI 410 [23,29].

Durmoo et al. [30] studied the tribocorrosion performance of AISI 304 stainless steel for an agricultural sugar and alcohol production industry application, where chloride levels of around 1300 ppm were found in the sugar cane juice. This corrosive condition was reproduced in the present study, as well as a less aggressive medium (pure water) as the corrosivity limit range representative of agribusiness segment applications. The tribocorrosion was explored in the additive stages of corrosion and erosion, aiming to reproduce operating conditions typical of equipment and structures involved in the agricultural process. To the best of our knowledge, this is the first work studying the erosive impact of corn particles. Camacho et al. [31] studied the erosion caused by rice grains for an aluminum application; Bahri et al. [32] performed similar work studying the impact of olive seeds against a AISI 304 stainless steel, but none studied erosion coupled with corrosion for a range of materials. However, most of the erosion-corrosion studies found were conducted using mineral particles as erodent [33–35]. In contrast, studies examining the mechanical damage caused by grains in contact with a metallic surface can be found more frequently [36,37], as it is a socially more relevant topic. Thus, this literature gap regarding erosion-corrosion due to grain action also stands as one of the main motivations for this work. Additionally, the adopted methodology is unprecedented and innovative in the study of mechanical and corrosive components characteristic of the agribusiness sector.

2. Methods

2.1. Materials characterization

A ferrite-martensite dual-phase UNS S41003 (11CrTT) steel, an austenitic AISI 304 (18Cr8Ni) stainless steel, a mild (ASTM A36) and an advanced high-strength carbon steel (AHSS) were studied. Carbon content in steels was measured via infrared absorption using a Leco CS444® and N via Leco TC436® thermal conductivity analysis equipment. All other elements were analyzed using ThermoARL 4460 optical emission spectrometry equipment. For the hardness evaluation, an Instron Wolpert Testor 930s machine was used, while a StruersDuramim 4 was used for the microhardness testing. For the metallographic analysis, samples were cut in a cooled abrasive disc machine and embedded in Bakelite polymeric resin using BUEHLER Simplimet1000® equipment. A Abramin® polisher from Struers was used to surface grinding in 120, 220, 320, 500 and 600 grit sandpapers. Finally, the samples were polished with Ø 9, 3 and 1 μm diamond paste and, finally, an optical microscope produced by the manufacturer Leica™ equipped with QWin Standard software was used for the microstructure analyses.

2.2. The test setup

The behavior of steels under pure corrosion, pure erosion and erosion-corrosion condition was evaluated by using the setup shown in the Fig. 1. For the corrosion test, a fog chamber (Salt-Spray Test [38]) from the manufacturer Equilam model SS1000e was used (Fig. 1a). The chamber temperature was fixed at 35 °C and the relative humidity on 95% for all the tests. An acrylic device was used to standard positioning and inclination angle between specimens. The pure corrosion and erosion-corrosion tests were realized in two different media: deionized water (electrical conductivity below 1 μS/cm.25 °C [39]) and 1300 ppm of chlorides containing (0.03 M NaCl) solutions. Through using aninoLab® pH/cond 700 device, a close to neutral pH (6.29) and an electrical conductivity of 0.402 μS/cm.25 °C was obtained for the deionized water solution while a slight acid pH (6.01) and an electrical conductivity of 6001 μS/cm.25°Cfor the chlorides containing solution.

A shot blasting equipment (CMV model 9075X) originally designed to operate with carbon steel shots was adapted to this work (Fig. 1b). Corn particles (crushed grains) were used as erodent to simulate their impact on the surface degradation of steels applied in agro-industrial metallic structures and equipment like chutes, conveyors, and distributors. The air jet equipment was maintained at a fixed pressure of 5 bars for all the tests. The assembly used allows adjusting parameters such as the attack angle, the distance, and the height of the nozzle from the sample surface (Fig. 1c). The flow valve was set fully open to ensure maximum erosive flow, and to eliminate the possibility of erodent recirculation, an auxiliary silo was adapted to the system. A metallic sample holder was built to accommodate the specimens, ensuring the reproducibility of their repositioning and the maintenance of test parameters throughout the erosion cycles, as well as avoiding damping or displacement of the sample during the shot blasting. This device was fixed to the structure of the cabinet, level with the floor. The angle of inclination of the pistol in relation to the sample was fixed at 35°, being the more aggressive angle, according to several authors [31,34]. The height and distance of the gun nozzle in relation to the sample surface were also fixed at 75 and 127 mm, respectively, as demonstrated in Fig. 1 d. A shot-blasting time of 60 s was fixed for all the erosive tests. The particle size distribution of the corn particles used was measured through standard particle size sieves. The morphology of the particles was observed by using a Zeiss Stereo Microscope anda FEI™ Quanta FEG250 Scanning Electron Microscope (SEM).

The samples for pure corrosion, pure erosion and erosion-corrosion tests were cut to 50 × 40 mm dimension using electrical discharge machine (EDM) technique. The surface preparation was standardized for all the samples aiming the leveling of the different topographies. A

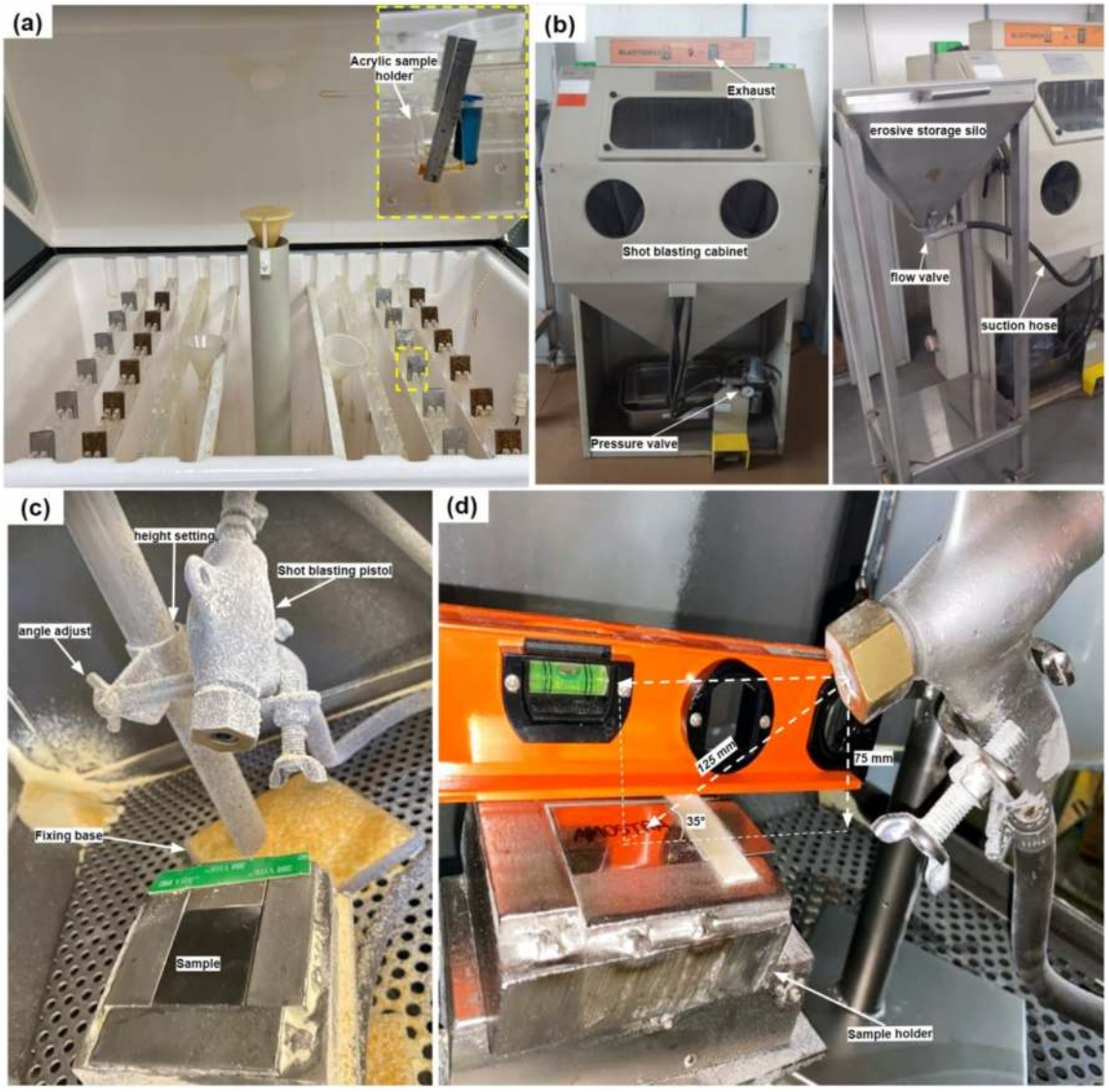

Fig. 1. Equipment used in corrosion and erosion tests: (a) salt-spray chamber with acrylic device for samples positioning, (b) shot blasting cabinet adapted for corn particles, (c) multi adjustable parameters pistol and (d) parameters adopted for erosive tests.

Phoenix 2000® rotative polisher and a sequence of sandpapers were used for this preparation. The procedure consisted of polishing the samples with 120 and 220 grit sandpapers for 180 s, followed by finishing for 300 s with 320 grit sandpaper for the upper face. The lower face and edges were grinded only with 120 grit sandpaper. After finishing the preparation, the samples were kept in a dryer with silica gel.

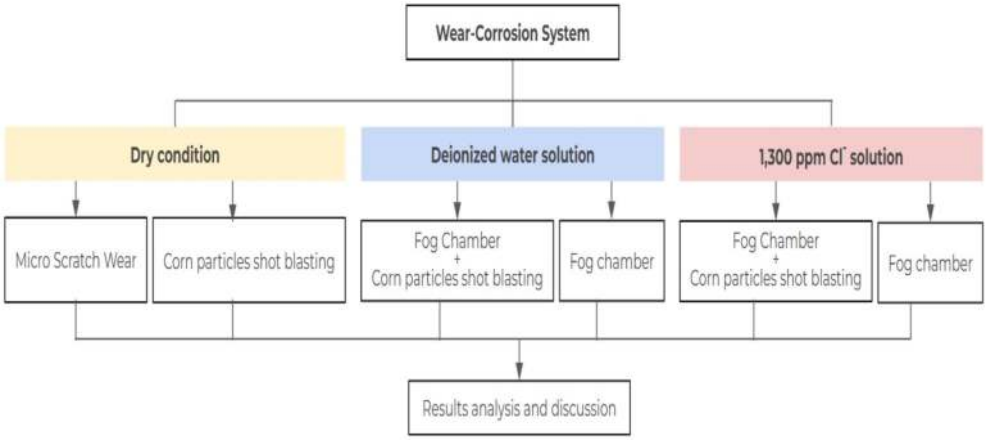

Fig. 2. Flowchart of tests to evaluate the erosion, corrosion, and erosion-corrosion resistance of steels.

Fig. 2 shows a flowchart representing the tests that each steel was subjected to.

2.3. Erosion-corrosion and pure corrosion tests

The structure of the pure corrosion and erosion-corrosion tests was defined based on a 24-h cycle of operation, to reproduce operating conditions close to those of agricultural equipment that is used in the field. Using the Sartorius microanalytical balance model MSA225S with a resolution of 0.01 mg the mass variation of the specimens was carried out throughout the daily cycles. Except for the pure erosion condition, 10 days of tests were carried out, summarizing 10 consecutive cycles of 24 h for each solution (deionized water and 1300 ppm of chlorides). For the pure erosion analysis, a single 600 s shot blasting test was carried out, and the samples were cleaned only by nitrogen blowing to remove the fine corn added (starch). The objective was to minimize as much as possible the exposure of samples to a humid atmosphere, especially the carbon steel ones, which could influence oxide formation and consequently mass variation.

In erosion-corrosion and pure corrosion tests, to concentrate the corrosive events in a controlled area of the samples, the lower face and edges of the erosion-corrosion and pure corrosion specimens were protected with an organic varnish (acrylic resin). Once removed from the fog chamber daily, the specimens were air-dried for 5 h of atmospheric exposure. For pure corrosion samples, the mass measurements were done daily after the air-drying step, while for erosion-corrosion samples, an additional measurement was done after the shot blasting step. Finally, to obtain the final mass loss, after 240 h of test, the pure corrosion and erosion-corrosion samples were successively cleaned in an ultrasonic bath with acetone to completely remove the varnish layer. For the carbon steels, a chemical cleaning of the oxides formed on the surface was needed to determine the real mass loss after the erosion-corrosion and pure corrosion tests. A bath of hydrochloric acid (HCl)-based solution with a corrosion inhibitor was used, according to the ASTM G1 [40] C.3.5 procedure. In addition to SEM-EDS (Energy Dispersive X-ray Spectrometer) and stereomicroscope analysis, the topography of pure erosion, pure corrosion and erosion-corrosion was evaluated before and after the tests using a Hommel-Etamic T8000 model profilometer equipped with Mountains Map software.

2.4. Scratch wear resistance

The scratch wear resistance of the materials was evaluated using a Micro Combi Tester – MCT3 Step 500 Anton Paar equipment with a Rockwell type diamond indenter of 100 μm of radius. A sliding speed of 2 mm/min and a 3 mm length scratch were performed without lubrication. Along with the metallic materials, a corn seed was also prepared in polymer resin and evaluated in a comparative way. The morphology of the scratch areas was evaluated by SEM analysis.

2.5. Mass loss and corrosion rates determination

The initial mass of the specimens was measured before and after the varnish layer had been applied, and this value was subtracted from the mass loss presented by the materials. It would have adopted three samples for each condition, generating an average mass loss rate and standard deviation results for each cycle. The Eq. (1) was used to calculate the mass loss over the pure corrosion and erosion-corrosion cycles.

$$\mathrm{MAccum} = \frac{\mathrm{mv0} - \mathrm{mvf}}{\mathrm{A}} \quad (1)$$

where M_{Accum} is the accumulated mass loss rate (mg/mm^2), m_{v0} and m_{vf} the initial and daily mass of the specimen coated with varnish (mg), respectively. Regarding pure corrosion samples, the m_{vf} was measured daily after the fog chamber while for erosion-corrosion samples after shot blasting cycle. The accumulated mass loss was updated each new cycle. A is the specimen working area (mm^2). After the varnish removal and chemical cleaning of the oxides, the Eq. (2) was used to determine the final corrosion rates of the materials.

$$\mathrm{CR} = \frac{\mathrm{KM_R}}{\mathrm{ATD}} \quad (2)$$

The term CR is the corrosion rate in mm/year, K the constant for mm/year conversion and M_R the real mass loss of the specimen (g) after varnish layer and oxides removal. A, T and D symbols are the area (cm^2), exposure time (hours) and steel density (g/cm^3), respectively. For the pure corrosion and erosion-corrosion rate calculation, a total time of 240 h was considered. A density value of 8.00 g/cm^3 was used for the austenitic stainless steel and 7.85 g/cm^3 for the ferritic-martensitic and carbon steels. An area of 20 cm^2 was considered for each specimen (5 × 4 cm dimension).

3. Results and discussion

3.1. Materials characterization

The results of chemical composition and Brinell hardness of the materials are shown in Table. The 18Cr8Ni is the most well-known and widely used stainless steel in the market, with excellent corrosion resistance due to the high contents of chromium and nickel, even though it presents a high cost [9]. The 11CrTT contains an optimized content of chromium and no nickel addition, maintaining a level of corrosion resistance suitable to several environments [41].

After quenching, along the good corrosion resistance, this alloy can reach high yield strength and hardness, maintaining good forming properties [42]. The ASTM A36 steel is the cheapest and most widely used structural carbon steel in the market, owing to their lower cost, good weldability, and favorable structural properties. The AHSS is an advanced material, widely used in applications that require wear resistance, such as in the mining sector. The boron, combined with the high carbon and other elements such as nitrogen and chromium, significantly increases hardenability, providing suitable mechanical properties [43]. The microstructures of the materials are shown in Fig. 3.

The 18Cr8Ni shows a microstructure of well recrystallized polygonal grains, as well as the occurrence of delta ferrite lines aligned in the austenitic matrix. Martensite islands can also be seen due to plastic deformation caused by mechanical polishing during the surface preparation process. For the 11CrTT steel, a dual-phase microstructure of ferrite and martensite is revealed, obtained after heat treatment and quenching. The occurrence of aligned delta ferrite lines is also observed. ASTM A36 steel presents a microstructure of ferrite and pearlite while AHSS steel reveals a homogeneous martensitic structure, with a highly refined grain size. Additionally, a region with grain morphology distinct from the rest of the matrix can be seen in a 15 μm thick layer on the surface of this steel, which corresponds to a decarburized region [10].

The apparent density of 0.699 g/cm^3 was determined for the corn particles based on the ASTM D1895 standard methodology. The particle size distribution (Fig. 3a), morphology (Fig. 3b), and surface characteristics (Fig. 3c) of the grains are shown in Fig. 4.

3.2. Scratch test

Fig. 5 presents the results of scratch wear test [44] carried out on the steels and corn kernel samples. For a constant load of 10 N applied, the penetration depth (Fig. 5a) and width (Fig. 5b) of the scratch in the corn surface was about 6 times greater when compared to the softer steel (A36). The advanced high-strength steel (AHSS) presented the lowest penetration depth and scratch width, showing the highest wear resistance among the materials and conditions tested. There is a direct relationship between the wear and scratch area and the mechanical

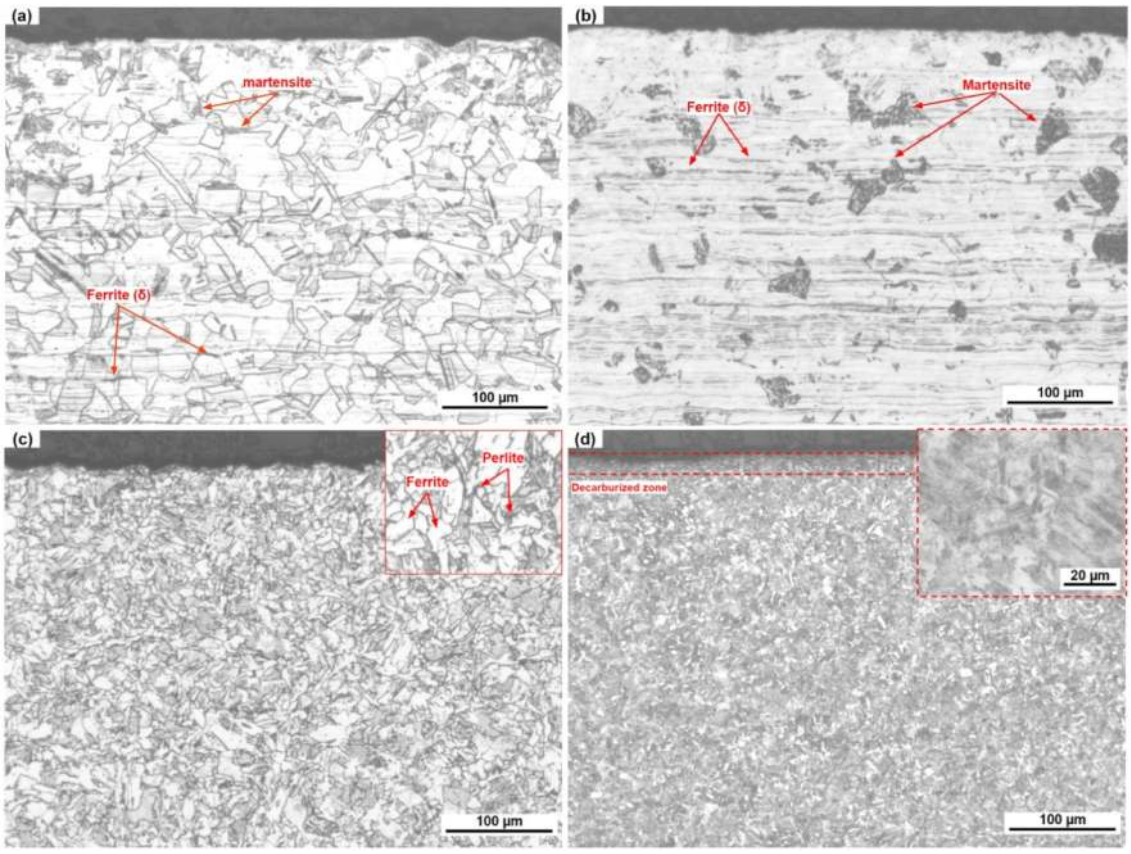

Fig. 3. Microstructure of the steels (a) 18Cr8Ni, (b) 11CrTT, (c) A36 and (d) AHSS near to the surface via optical microscope (chemical etchings with Aqua Regia, Vilella, and Nital).

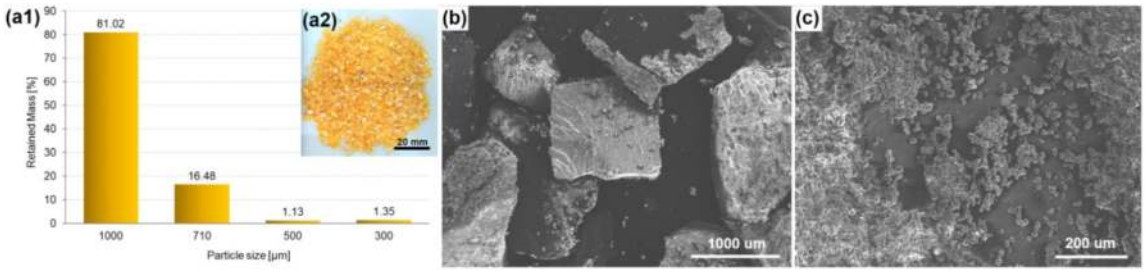

Fig. 4. Corn particles (a1) size distribution, (a2) visual aspect, (b) morphology and (c) surface detail via SEM.

properties of the materials, such as hardness. The SEM micrographs of the 18Cr8Ni (Fig. 5c), 11CrTT (Fig. 5d), A36 (Fig. 5e) and AHSS (Fig. 5f) surface steels shows a grooving area and the occurrence of material displacement in the edges (pile-ups area). The 18Cr8Ni austenitic stainless steel presented cracks in the bottom of the scratch, probably associated with the martensitic transformation induced by the plastic deformation caused by the tip sliding, which is characteristic of this alloy [45,46]. This phenomenon increases the steel's mechanical properties but can be deleterious for corrosion and wear resistance [47]. To accommodate the tangential force imposed by the hard tip motion against the matrix, the corn surface evolves cracks preexistent, displacing less mass in the edge regions if compared with the steels. The AHSS steel presented the lowest penetration depth and scratch width, showing the highest wear resistance among the materials studied.

3.3. Pure erosion resistance

Fig. 6 shows the mass loss of the steels after a single shot blasting of 600 s with corn particles. Fig. 7 shows the surface of the steels before and after shot blasting with corn particles.

It is possible to verify by the magnitude of the measured mass variations (10^{-5} mg/mm^2) that the particles did not present energy to remove a significant amount of mass from the surface of the steels. These particles, in line with micro scratching results analysis, did not present mechanical properties to overcome the elastic resistance of metallic surfaces. However, it is still possible to observe coherence in the pure erosion results. 11CrTT stainless steel showed a lower mass loss rate compared to 18Cr8Ni steel, which can be associated with its greater hardness. The A36 and AHSS carbon steels showed a mass gain (10^{-5} mg/mm^2) which in turn already reinforces a mass loss very close to zero in pure erosion test. Despite the samples being stored in a dryer container with silica gel until shot blasting, it is suggested that this mass gain is associated with oxide formation due to the period of external atmosphere exposition during handling. However, the SEM analysis revealed some subtle changes in the surface of the materials, such as a smoothing effect after erosion. The presence of burrs on the polished

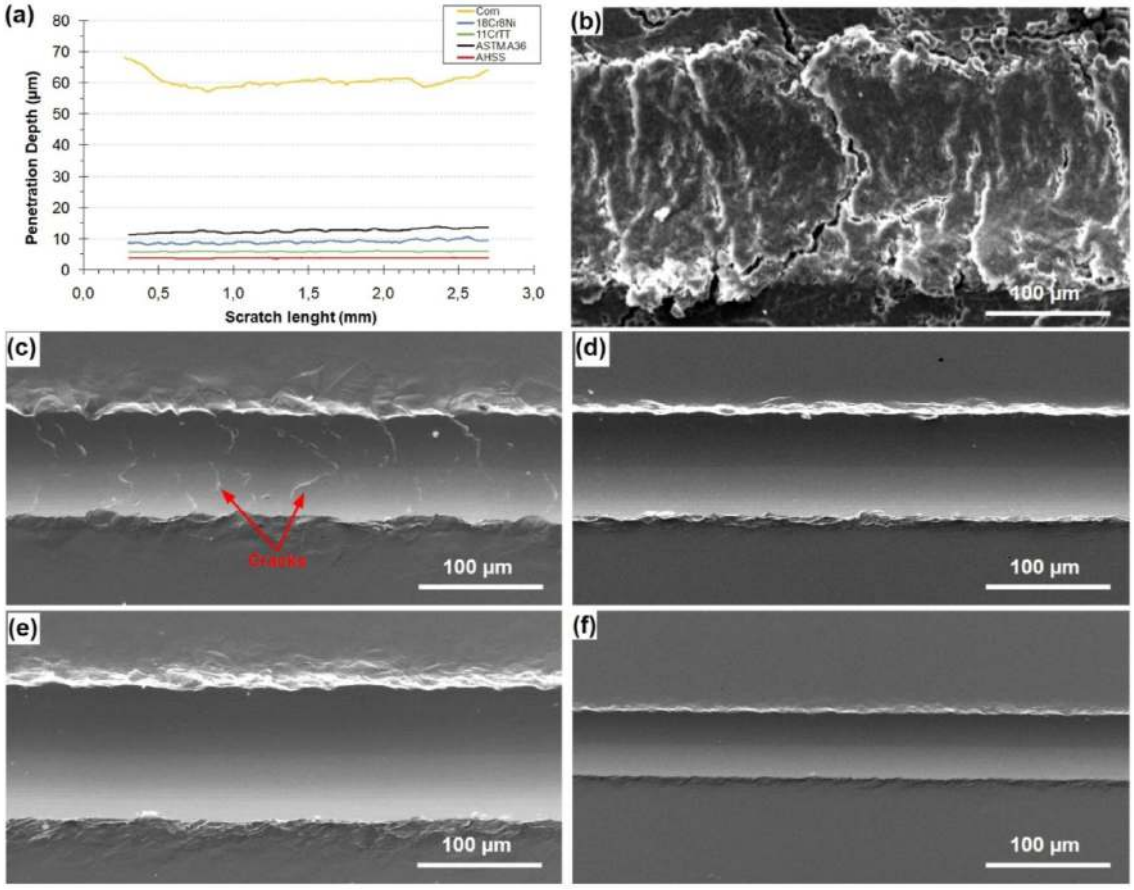

Fig. 5. Results of comparative (a) penetration depth and morphology of the scratch for (b) corn seed, (c) 18Cr8Ni, (d) 11CrTT, (e) A36 and (f) AHSS steels via SEM after scratch wear test with constant load of 10 N and diamond tip with radius 100 µm.

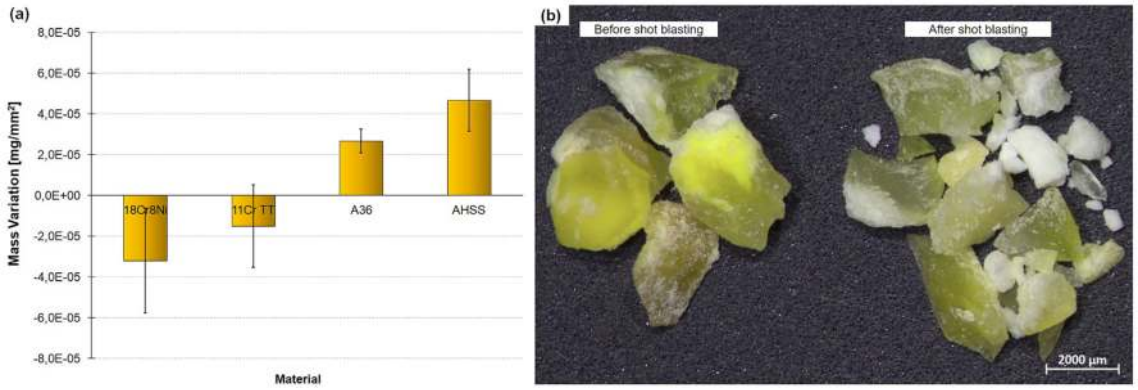

Fig. 6. Results of (a) mass loss rate of the materials and (b) corn particles broken after pure erosion test.

surfaces of the steels 18Cr8Ni (7a), 11CrTT (7b) and A36 (7c) was identified. However, it appears that with blasting, most of these non-detached deformed particles was removed, softening the surface. For AHSS steel, this characteristic was not observed.

With the aim of investigating possible mechanical changes resulting from the action of corn particles, microhardness tests were carried out on samples before and after shot blasting. The obtained results, presented in Table 2, did not indicate significant changes for all materials. Despite the small values of mass loss and the absence of changes in the mechanical properties of the materials, the study of roughness and topography in turn indicated important changes after pure erosion.

Table 3 presents the roughness of the samples before and after the pure erosion test. The A36 carbon steel had its surface more grooved by the grains of silicon carbide (SiC) present in the sandpapers used in the surface preparation, resulting in a higher starting roughness. In this way, the AHSS steel, the hardest material, showed the lowest initial roughness. However, after shot blasting, except for AHSS steel, all materials showed lower roughness with less dispersion in the results.

The corn particles were not able to deform the metallic surfaces, remove mass by wear or even cause a hardness change; however, they were able to act in the topographical heterogeneities present on the surfaces. This phenomenon of surface smoothing can be associated with the average height of peaks reducing and can be beneficial to the materials once a less rough surface tends to have greater corrosion

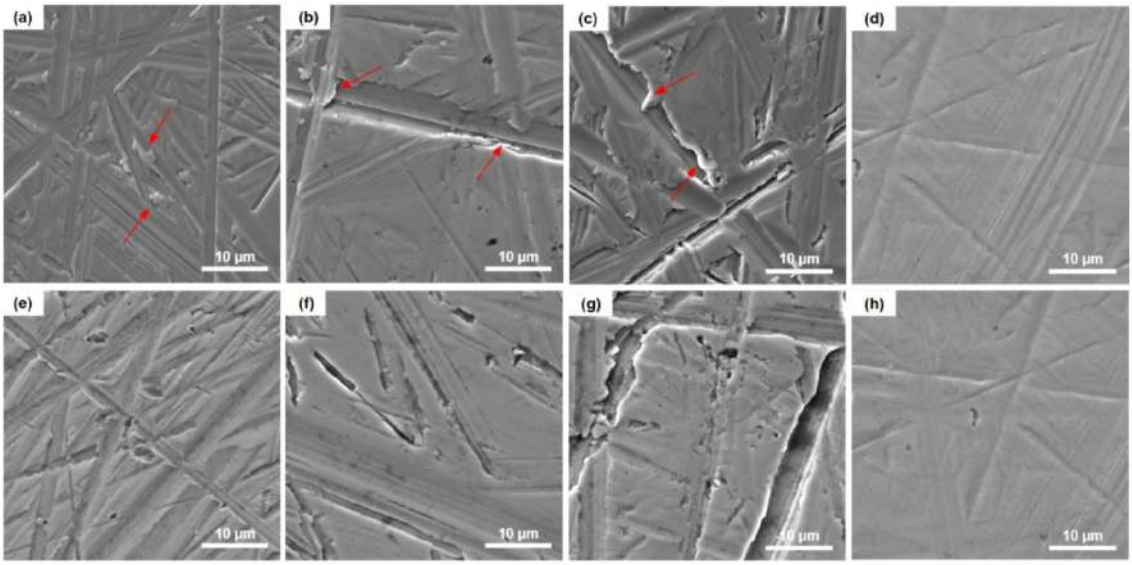

Fig. 7. Surface of the steels 18Cr8Ni, 11CrTT, A36 and AHSS via SEM,respectively, (a,b,c,d) before and (e,f,g,h) after shot blasting with corn particles.

Table 1
Chemical composition (wt.%) and hardness (HB) of the materials.

Element	C	Mn	Si	Cr	Ni	Mo	Cu	Nb	Fe	N [ppm]	B [ppm]	Brinell Hardness
18Cr8Ni	0.035	1.252	0.451	18.156	8.099	0.169	0.262	0.014	bal.	449	–	178 ± 2.0
11CrTT	0.014	0.509	0.465	11.067	0.338	0.013	0.035	0.037	bal.	158	–	286 ± 2.5
A36	0.139	1.027	0.180	0.011	0.012	0.005	0.011	0.001	bal.	35	6	152 ± 2.9
AHSS	0.231	0.794	0.286	0.972	0.030	0.146	0.021	0.011	bal.	52	14	507 ± 6.3

Table 2
Microhardness before and after 600 s of shot blasting with corn particles (HV100).

Condition	18Cr8Ni	11CrTT	A36	AHSS
Before Erosion	236 ± 10.8	338 ± 5.5	177 ± 7.3	610 ± 11.1
After Erosion	240 ± 2.2	333 ± 12.4	184 ± 7.5	606 ± 17.6

Table 3
Materials surface roughness before and after 600 s of shot blasting with corn particles (µm Ra).

Condition	18Cr8Ni	11CrTT	A36	AHSS
Before Erosion	0.074 ± 0.05	0.073 ± 0.04	0.202 ± 0.07	0.034 ± 0.01
After Erosion	0.022 ± 0.01	0.026 ± 0.01	0.067 ± 0.01	0.045 ± 0.01

resistance, as a rougher surface is more likely to be corroded [48,49]. However, in the case of applications involving carbon steels exposed to a naturally humid external atmosphere, such as agribusiness, corrosion will be present, and the microscopic profile of the surface will be drastically modified.

3.4. Pure corrosion resistance

3.4.1. Mass loss analysis

The mass loss of the 18Cr8Ni and 11CrTT stainless steel under the pure corrosion condition was close to zero after the varnish layer removal (10^{-4} mg/mm^2). However, slight mass loss measurements were observed for these steels while coated with varnish during the daily cycles, which could be associated with the varnish degradation. Despite the low magnitude of the variations (10^{-3} mg/mm^2), the varnish loses mass over time, probably due to the cyclic exposition to the fog chamber atmosphere [50]. In this way, the mass loss curve of the varnish was determined, assuming the same behavior of this compound in stainless steel and carbon steel specimens. Fig. 8 shows the A36 and AHSS fitted mass variation curve over 10 cumulative cycles of pure corrosion in deionized water and 1300 ppm of chloride solutions. A mass gain is observed for all the carbon steel samples, which can be attributed to the rust growth. However, if all the mass gain was associated to the rust formation, this momentary gain would be converted into future effective mass loss. Garcia et al. [51] reported in their study that for carbon (0.23% C) and weathering (0.13% C – 0.47% Cr) steels, around 45–47% of the corrosion products are lost, and only 21% of the corroded iron converts completely into adherent rust. This information was confirmed later by other authors [52]. In the deionized water media, the carbon steels exhibit better corrosion performance than in the chloride solution, as expected. The AHSS showed a 2.68 times lower mass gain rate compared to the A36 steel (0.019 and 0.051 mg/mm^2, respectively) in the deionized water. Furthermore, the AHSS enters a stability mass variation regime from the 6th cycle in these media, which could be associated with the presence of chromium [53].

This behavior can be better observed in Fig. 8b, where is detailed the mass loss curve of these steels in the deionized water media. In the 1300 ppm chloride medium, the mass gain rates for the AHSS and A36 steels were similar and significantly higher when compared to the deionized water media (0.268 and 0.286 mg/mm^2, respectively). The values represent a performance worsening of around 14.10 times for the AHSS and 5.61 for the A36 steel. The steel's mass variation rates increased continuously over time, which also indicates that it is difficult to reach a stability regime despite the surface being totally covered by oxide layers, indicating the nature of the less protective rust formed by these steels in the saline medium.

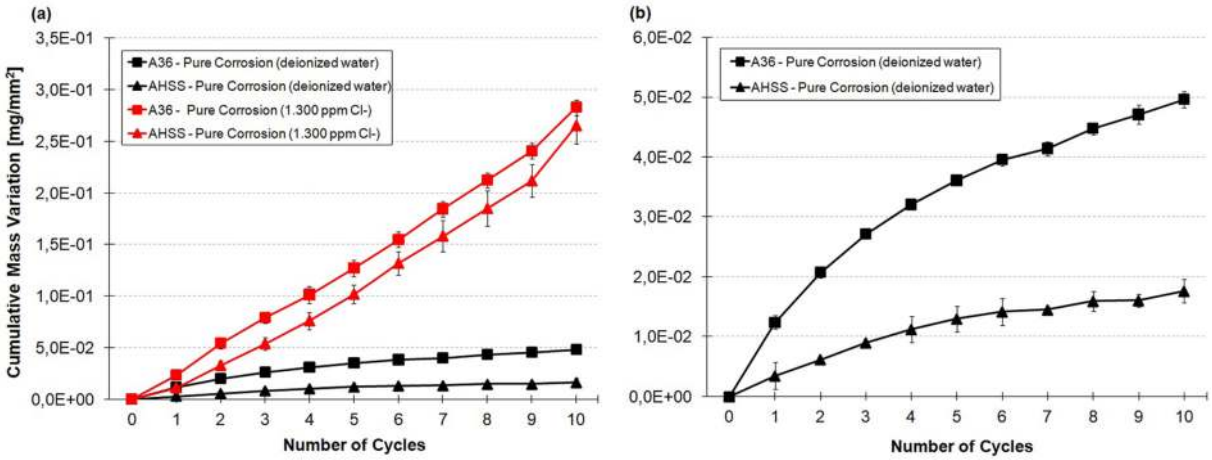

Fig. 8. Mass loss rate behavior of A36 and AHSS carbon steels in pure corrosion: (a) deionized water and 1300 ppm of chlorides media comparative and (b) deionized water medium in detail.

3.4.2. *Surface analysis*

Fig. 9 shows the surfaces after 10 cycles (240 h) of pure corrosion in deionized water and in the 1300 ppm chloride solution. The 18Cr8Ni and 11CrTT surfaces remained completely preserved in the deionized water medium (Fig. 9a), as expected. In the solution with 1300 ppm of chlorides (Fig. 9b), however, both steels presented a slight yellowing aspect with the presence of orange color stains, which indicates the presence of iron oxides. It can also be seen the presence of corrosion products added at the 11CrTT sample edges. These are regions of higher energy and corrosive solution stagnation due to the orientation of the samples in the chamber. The SEM analysis indicated the presence of scattered oxide points on the 18Cr8Ni surface (Fig. 10a) and the presence of advanced localized corrosion points (pitting) on the 11CrTT surface (Fig. 10b). The 11CrTT worst performance is coherent with their low chromium content, which tends to corrode faster compared to an 18% chromium alloy in an environment containing a high content of chlorides. Concerning carbon steels, it is possible to observe in the deionized water (Fig. 9a) a larger fraction of areas with the initial surface exposed to the solution of the AHSS steel when compared to the A36 steel. In the media containing chlorides (Fig. 9b), both steels have a surface completely covered by layers of a thick rust. In both media, but more visible in the deionized water, the formation of two main oxide layers with distinct characteristics was observed, with a very similar aspect in both steels. Fig. 11 shows the morphology of these layers analyzed by using a stereomicroscope.

In atmospheric corrosion, the oxide coating formed is generally bulky, porous and made up of different layers, without the necessary properties to protect the steel from the environment, such as passive oxide films [51,54]. Regarding non-adherent rusts, García and other authors [51,52,55] find that 3–18% of the iron mass is converted and

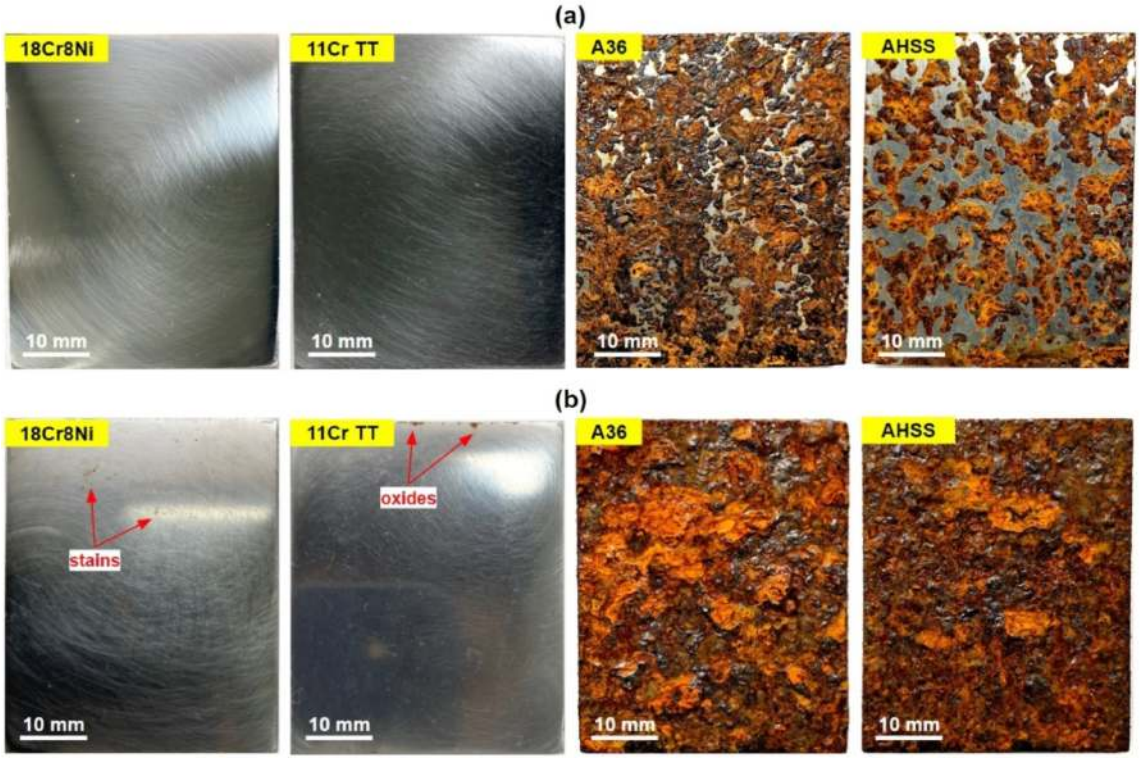

Fig. 9. Materials after 10 cycles (240 h) of pure corrosion in (a) deionized water and (b) 1300 ppm of chlorides solution.

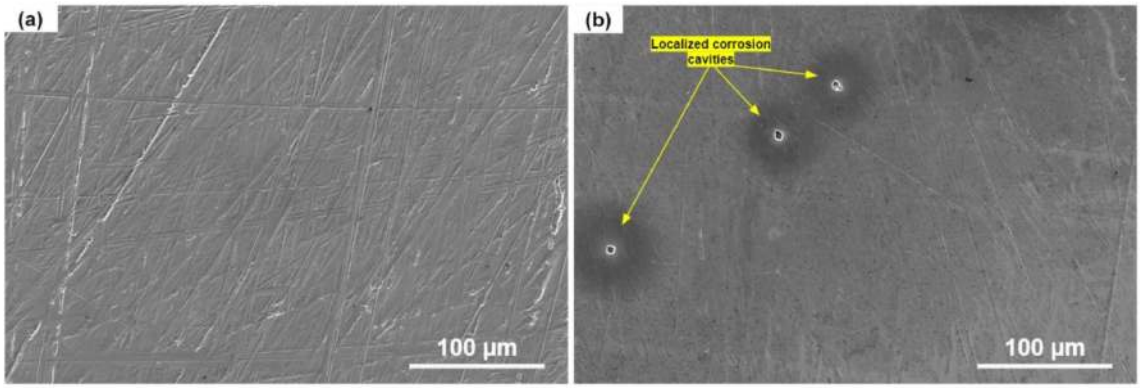

Fig. 10. Surface of the (a) 18Cr8Ni and (b) 11CrTT stainless steels via SEM after 10 cycles (240 h) of pure corrosion in 1300 ppm of chlorides media.

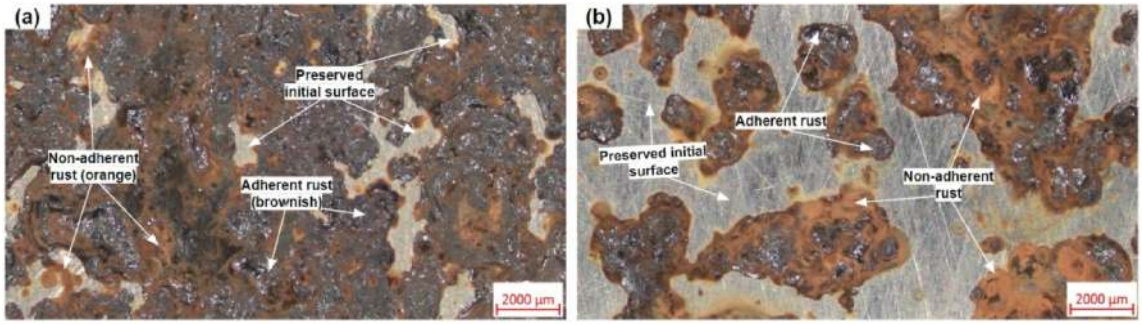

Fig. 11. –Surface of the (a) A36 and (b) AHSS carbon steels after 10 cycles (240 h) of pure corrosion in deionized water media via stereo microscope.

this layer, independent of the exposure times and chloride concentrations studied, are composed of lepidocrocite, goethite, hematite, and traces of akaganeite. The adherent rust was composed of lepidocrocite, spinel phase, goethite and akaganeite. In wet environments containing chlorides, iron and steel corrode, forming rusts with brownish colors [54] and this can be observed on the surface of both steels for the more

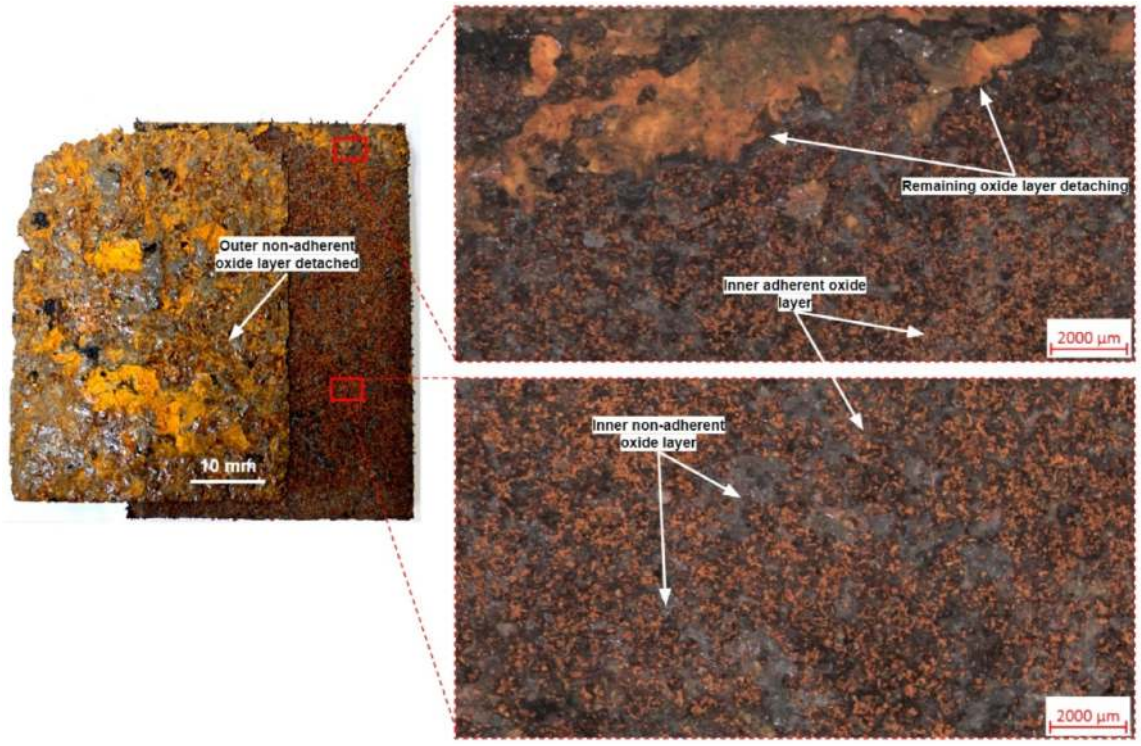

Fig. 12. Surface of the AHSS carbon steel after 10 cycles (240 h) of pure corrosion in 1300 ppm of chlorides solution presenting a detachment of outeroxide layer, due to handling after the final of the test.

internal layer. Above the referred brownish layer, a distinct external rust layer was identified, orange, with a less dense appearance and adhesion. This layer has a very similar characteristic to the non-adherent external layer formed in deionized water, however with a more brittle and porous appearance. In the case of weathering steels, an internal and adherent layer of corrosion products protects the steel from complete degradation. Fig. 12 shows a specimen of AHSS carbon steel at the end of the pure corrosion test, where a complete detachment of the external oxide layer formed is observed.

According to the literature, for steels constantly exposed to water, rusts keep growing and finally detach as flakes or even as slabs at the substrate/rust interface [54], which corroborates with the previous analysis regarding the non-adherent nature of these corrosion products.

3.5. Erosion-corrosion resistance

3.5.1. Mass loss analysis

For the erosion-corrosion tests, the mass loss presented by the 18Cr8Ni and 11CrTT stainless steels were close to zero (10^{-4} mg/mm^2 magnitude) compared to the carbon steels. Fig. 13 shows the A36 and AHSS fitted mass variation evolution, over 10 cumulative cycles of erosion-corrosion tests in deionized water and 1300 ppm of chlorides solutions. For both carbon steels, the mass removed in erosion-corrosion was very close to the mass theoretically gained in pure corrosion, reproducing a very similar curve shape. This observation aligns with the discussions established previously, in which the direct removal of mass by the impact of corn grains was considered of low relevance. In erosion-corrosion, it was easier for materials to reach a level of stability in deionized water, as can be seen in Fig. 13b. The AHSS showed a 2.23 times lower mass loss rate compared to the A36 steel (0.017 and 0.038 mg/mm^2, respectively). However, whether in pure corrosion or erosion-corrosion, it appears that AHSS steel clearly presents a severely impaired performance in more corrosive environments, such as in the presence of chloride ions [11].

In the medium containing 1300 ppm of chlorides, the mild and high-advanced carbon steels performed very close in terms of mass loss (0.227 and 0.256 mg/mm^2, respectively). A performance worsening of 6.74% was observed in the saline medium for the A36 steel while an increase of 13.35 times in mass loss was observed for the AHSS.

3.5.2. Surface analysis

Fig. 14 shows the 18Cr8Ni, 11CrTT, A36 and AHSS steel surfaces during the first erosion-corrosion cycle in deionized water medium: after the fog chamber cycle (Fig. 14a) and after 60 s of shot blasting with corn particles (Fig. 14b). In Fig. 15, the same surfaces are shown after 10 cycles of erosion and corrosion. The 18Cr8Ni and 11CrTT surfaces remained intact, maintaining their initial shine and mirrored appearance. In the case of A36 and AHSS carbon steels, it is clear that most of the poor or non-adherent oxides (orange color) were removed by the corn particles, which in turn were not able to remove the brown-colored oxides, which were more adherent [54].

Xu et al. [8,15] found similar results for the erosion-corrosion test of X65 carbon steel used for pipelines. It is suggested that most of the mass lost by these steels in each erosion-corrosion cycle is attributed to the removal of non-adherent oxides, establishing a condition of erosion-enhancing corrosion [15]. It is also observed that after the first cycle in the fog chamber (Fig. 14a), the surface of the carbon steels presents a large part of their area covered by oxides. However, over the cycles, the re-formation of orange-colored oxides (non-adherent [54]) is observed only in small localized areas of the surface (Fig. 15a). It is suggested that these points are restricted to regions where localized detachment of adherent oxides occurred due to the impact of the solid particles, where the base metal is more prone to oxidation. In this way, the stability level of mass loss reached by steels observed in the 6th erosion-corrosion cycle is clarified. The whitish color observed on the surface of the A36 samples can be attributed to corn fines (starch), released with the grains breaking, which adhered and were compacted in the porous structure of the external oxide layers throughout the erosion cycles. For AHSS steel, this was not observed, possibly due to the smaller amount of these oxides formed on the surface. The AHSS preserves a significant fraction of its initial surface free of oxides, like that observed for pure corrosion in deionized water. A localized corrosion mechanism was identified, with deeper and sparser cavities being formed. In the other hand, A36 steel corrosion is widespread on the surface, where localized cavities are also observed but smaller (Fig. 16). Although the role of chlorides in the initiation of pitting corrosion has long been known, only recently has this mechanism been shown to be more complex and also affect carbon steels, generating localized defects [14].

Xu et al. [8] observed that the erosion by silica particles in a NaCl solution leads to a change in the corrosion mechanism of the X65 carbon steel. The authors report a transition from generalized to localized corrosion mode, resulting in the formation of more stable pits and negative erosion-corrosion synergy, reducing the material's corrosion rate. Fig. 17 shows the surface of the materials at the end (10 cycles) of the erosion-corrosion test in a solution containing 1300 ppm of chlorides, just after leaving the fog chamber (Fig. 17a) and after 60 s of shot blasting with corn particles (Fig. 17b). Similarly to what was observed for deionized water, the surface of the 18Cr8Ni and 11CrTT steels maintained their shiny appearance, with some stains but no visible

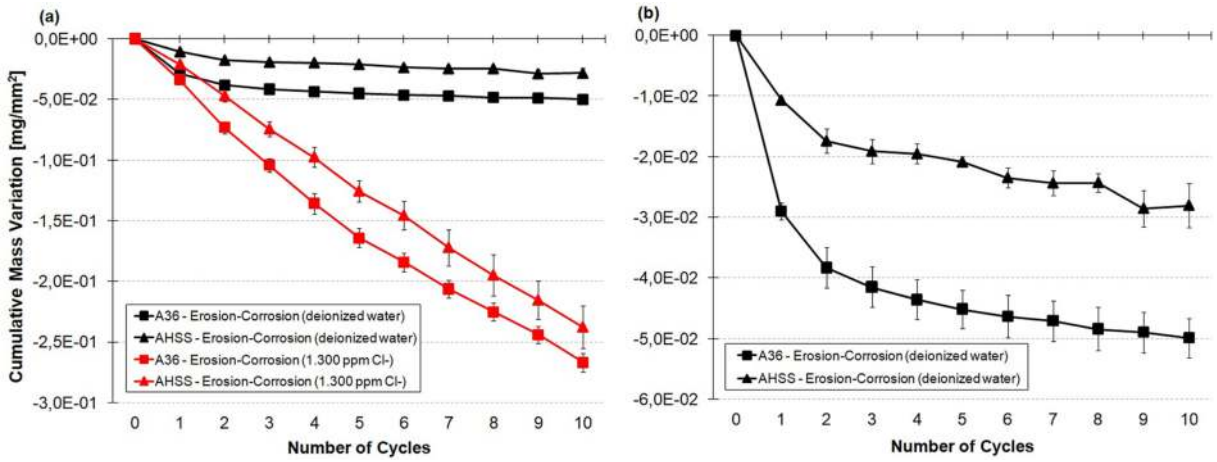

Fig. 13. Mass loss rate behavior of A36 and AHSS carbon steels in erosion-corrosion: (a) deionized water and 1300 ppm of chlorides media comparative and (b) deionized water media in detail.

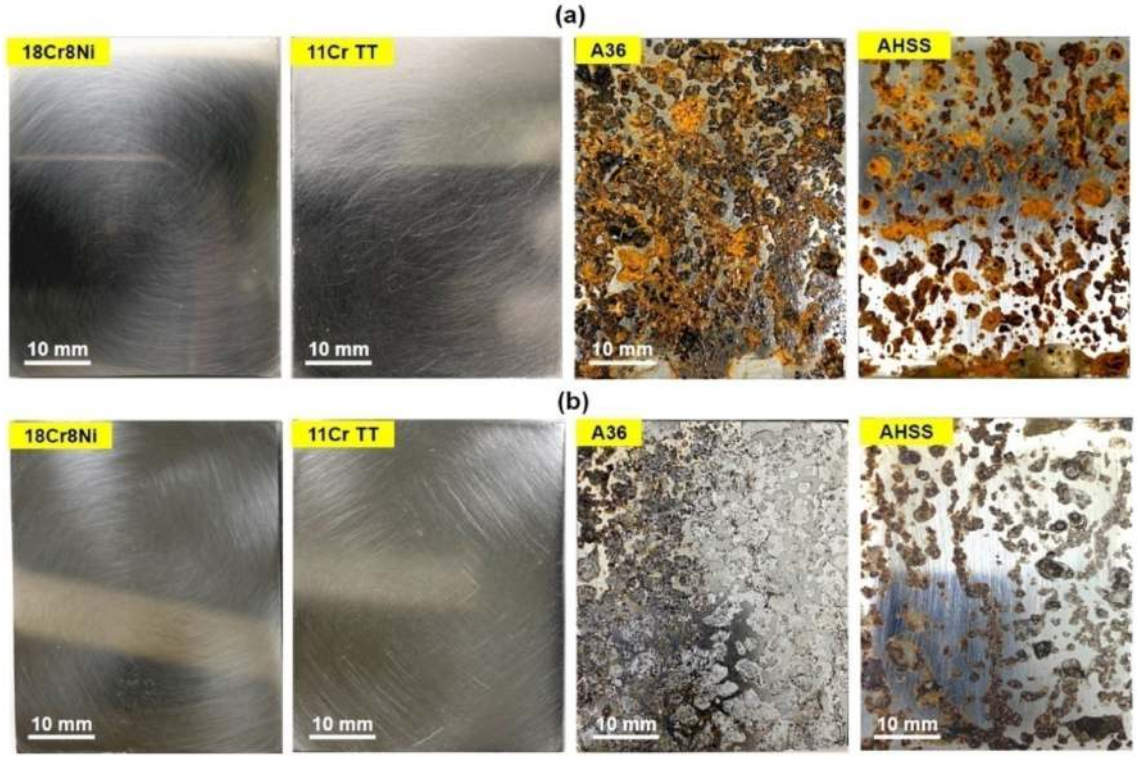

Fig. 14. Materials at the first cycle of erosion-corrosion in deionized water media: samples surface after the first (a) 15.5 h on the fog chamber and same surface after (b) 60 s of shot blasting with corn grains.

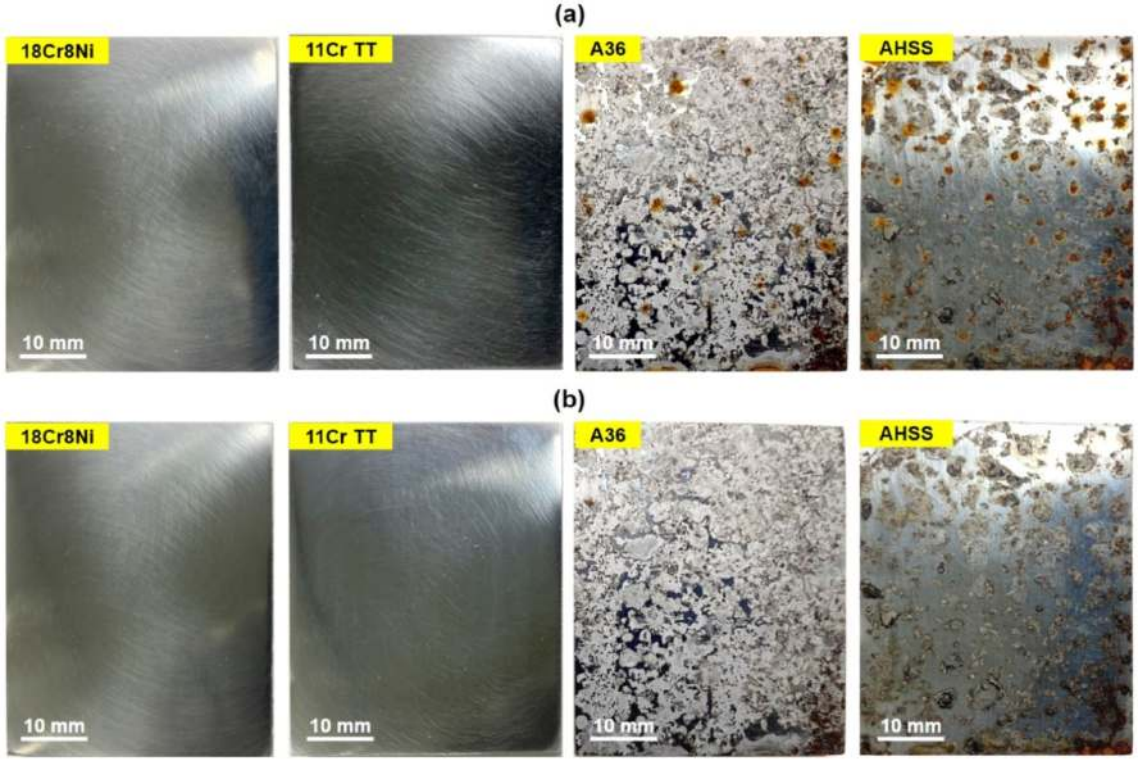

Fig. 15. Materials after 10 cycles of erosion-corrosion in deionized water: samples surface after (a) last 15.5 h on the fog chamber and the same surface after (b) 60 s of shot blasting with corn grains.

corrosion products. In the pure corrosion condition, the SEM analysis showed large pitting cavities in the 11CrTT, however, in erosion-corrosion with the polishing and periodic cleaning of the surface, this condition was restricted to stains. The grain impact hindered the progress of corrosion mechanisms under deposit, keeping the surface free of fouling and non-adherent corrosion products. In the other

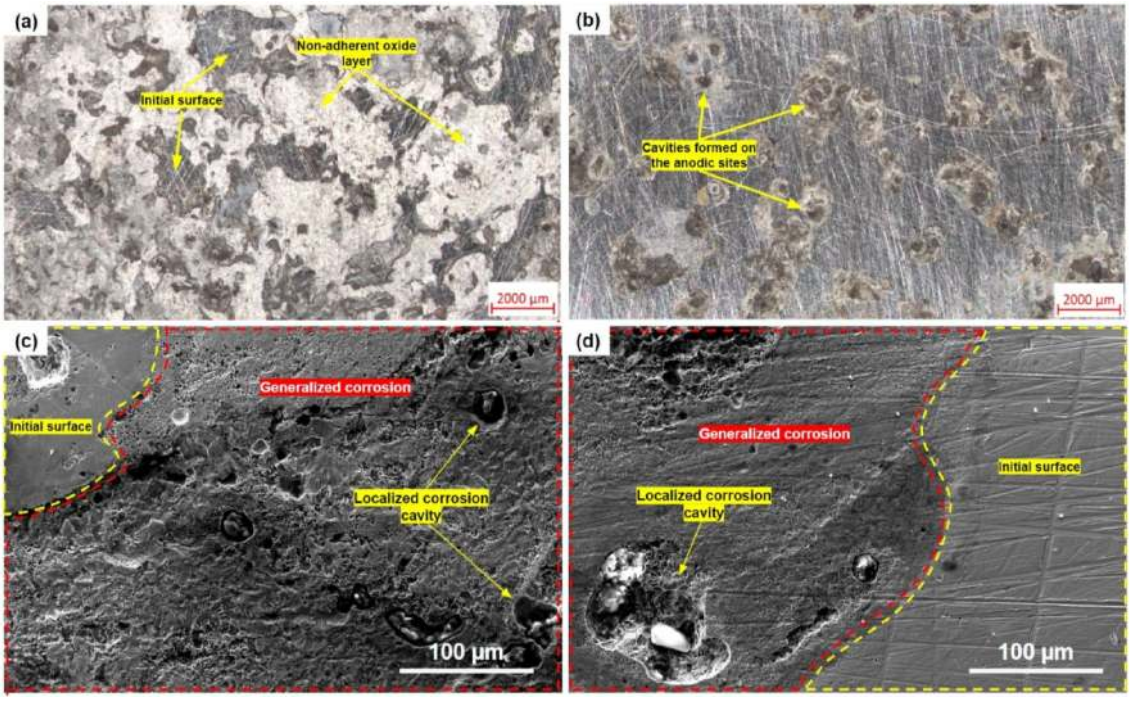

Fig. 16. Surface of the (a,c) A36 and (b,d) AHSS carbon steels via stereo and electronic microscope (SEM), respectively, after 10 cycles (240 h) of erosion-corrosion in deionized water medium.

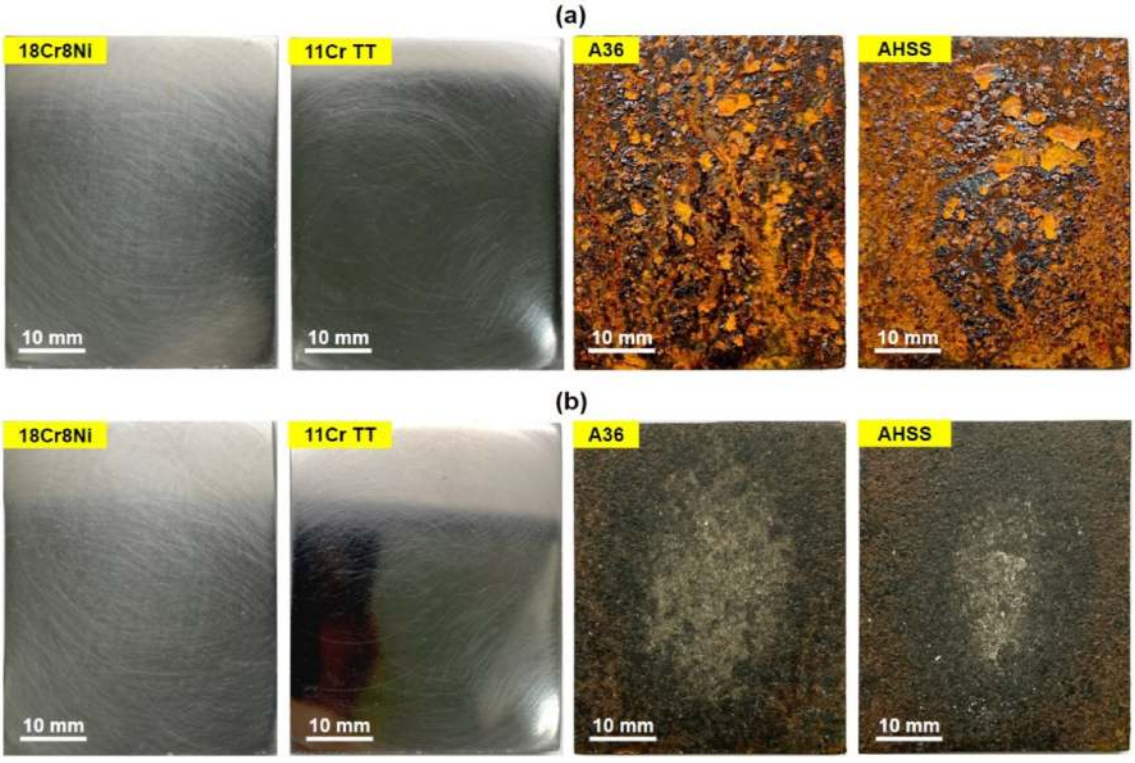

Fig. 17. Materials after 10 cycles of erosion-corrosion in 1300 ppm chlorides media: samples surface after (a) last 15,5 h on the fog chamber and same surface after (b) 60 s of shot blasting with corn grains.

hand, this phenomenon can also damage the passive film of the stainless steel, making the surface more susceptible to localized corrosion in aggressive environments, such as in the presence of chloride ions [6,23]. The A36 and AHSS carbon steels in the fog chamber form rusts, which are removed from the surface by the solid particles and represent the main mechanism of mass loss of these steels in erosion-corrosion.

AHSS steel forms less amount of rust in the wet cycles, therefore presenting lower mass loss rates during the shot blasting. The whitish appearance of the surface, attributed to the compaction of the corn fines generated, was concentrated in the central region of the samples, where

the erosion was more intense. Fig. 18 shows the A36 and AHSS steel surfaces after erosion-corrosion in the 1300 ppm of chloride solution analyzed by using the stereoscopy and SEM analysis.

Both steels presented a very similar surface after erosion-corrosion, and an enhanced galvanic corrosion mechanism was observed, explained by the continuous exchanging of anode and cathode sites in the surface, which some recent studies attribute to the effect of accumulated Fe_3C networks [8,15,56]. Because of the continuous removal of non-adherent corrosion products by the erosive agent necessary for inducing pitting, the effect of chloride can also be associated with the higher media conductivity, allowing for faster charge exchange and accelerating corrosion [14]. SEM-EDS analysis revealed the presence of residues inside cavities on the surface of both steels, presenting high contents of carbon and chlorine in their composition. These elements can be associated with corn residues (carbon-based), which, once trapped on the surface due to their porous and hygroscopic nature, were soaked in the solution with high chlorine content throughout the corrosive cycles. The chlorine levels far exceed the concentration present in the corrosive solution used, reaching values of around 25,000 ppm of this element.

3.6. Surface and corrosion rate analysis after oxides cleaning

Fig. 19 presents the corrosion rates in mm/year (logarithmic scale) obtained for 18Cr8Ni, 11CrTT, A36 and AHSS steels after pure corrosion and erosion-corrosion tests, for deionized water (Figs. 19a), 1300 ppm of chlorides medium (Fig. 19b). Obviously, after pickling, carbon steel loses even more mass, which is associated with adherent layers of rust not removed previously. The chloride-containing medium was considerably more aggressive than the steels in terms of mass loss. Interestingly, the pure corrosion condition was responsible for the highest corrosion rates, which was more evident in the deionized water media for the carbon steels. The damage was mitigated when the two factors acted together, creating a negative synergy [28]. The erosion-corrosion surface smoothing process reduced the corrosion rates, since a less rough surface is less electrochemically active [48]. An exception to this behavior was the 18Cr8Ni steel, whose corrosion rates were the lowest among the materials.

In general, the porous and non-adherent oxides formed on the surface of A36 and AHSS steels does not play a protective role in the solutions studied, since when periodically removed, erosion-corrosion represented a significant performance improvement. According to Tamura [54], the presence of rusts can accelerate carbon steel corrosion, where rusts are not corrosion-protective but corrosion-promoting. In the case of operation in aggressive media, such as in the presence of chlorides, these oxides retain the aggressive elements in contact with the metal surface, creating conditions of even greater corrosiveness at the interfaces. In the presence of erosion-corrosion, the less adherent rust layers formed are continuously removed, reducing this phenomenon's impact. Kayali et al. [57] found that ferrite-pearlite steels had a lower corrosion rate compared to a boronized dual-phase steel (0.15%C without Cr) in 3.5% NaCl solution, where the corrosion resistance decreased with increase in the martensite ratio. This result was verified in the present work, where AHSS had a worse performance (2.97 mm/y) compared to A36 steel (2.77 mm/y) under pure corrosion conditions. However, in the presence of corn particles, AHSS consistently performs better compared to A36, showing corrosion rates 30% lower.

The 11CrTT stainless steel with low chromium content, despite drastically lower corrosion rates compared to carbon steels, showed similar behavior, reaching higher corrosion rates in the pure corrosion condition ($3x10^{-3}$ mm/y in the 1300 ppm of chlorides media) than in the erosion-corrosion condition. Interestingly, in the case of 18Cr8Ni steel, due to the formation of an adherent and compact oxide film that effectively protects the metal, a higher corrosion rate was observed in the erosion-corrosion condition. The impact of the corn particles may have impaired the formation of the passive layer [58,59] and this hypothesis is reinforced by the significant increase in the erosion-corrosion rate from $2x10^{-4}$ mm/y in the deionized water to $9x10^{-4}$ mm/y in the 1300 ppm of chloride media. López et al. [29] also studied the erosion-corrosion of 18Cr8Ni and 0.13Cr stainless steels in a 3.5% NaCl solution in the presence of quartz particles. The authors found that erosion damage was predominant for the austenitic steel, while

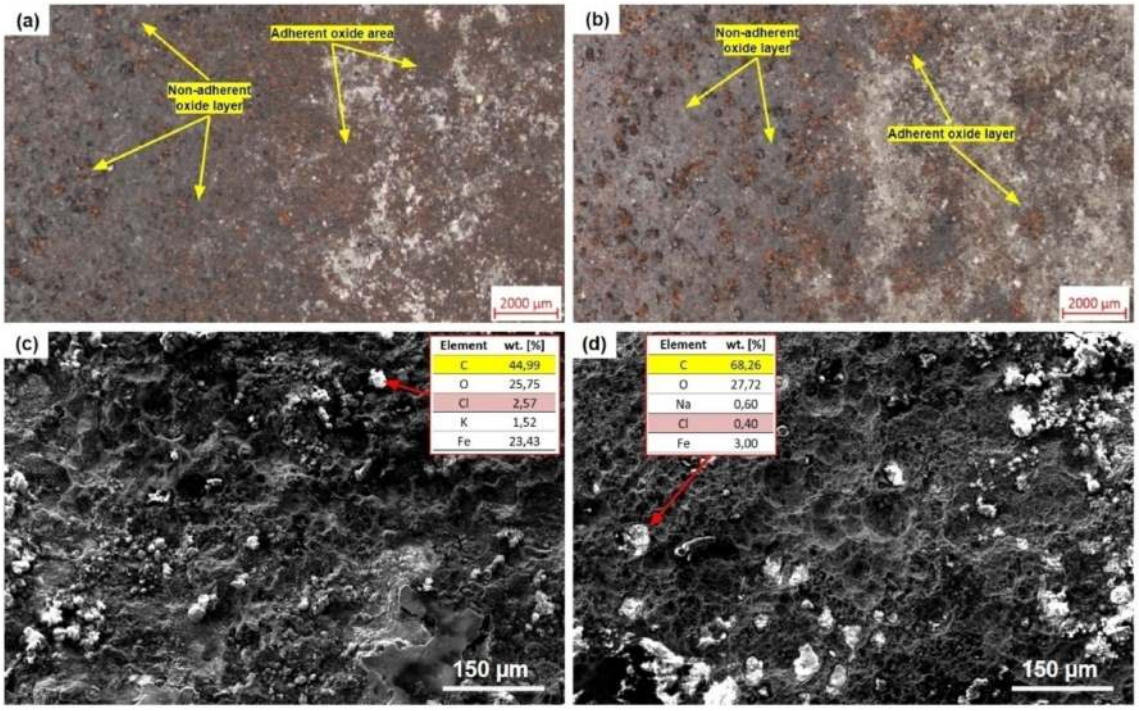

Fig. 18. Surface of the (a,c) A36 and (b,d) AHSS carbon steels via stereo and electronic microscope (SEM), respectively, after 10 cycles (240 h) of erosion-corrosion in 1300 ppm of chlorides media.

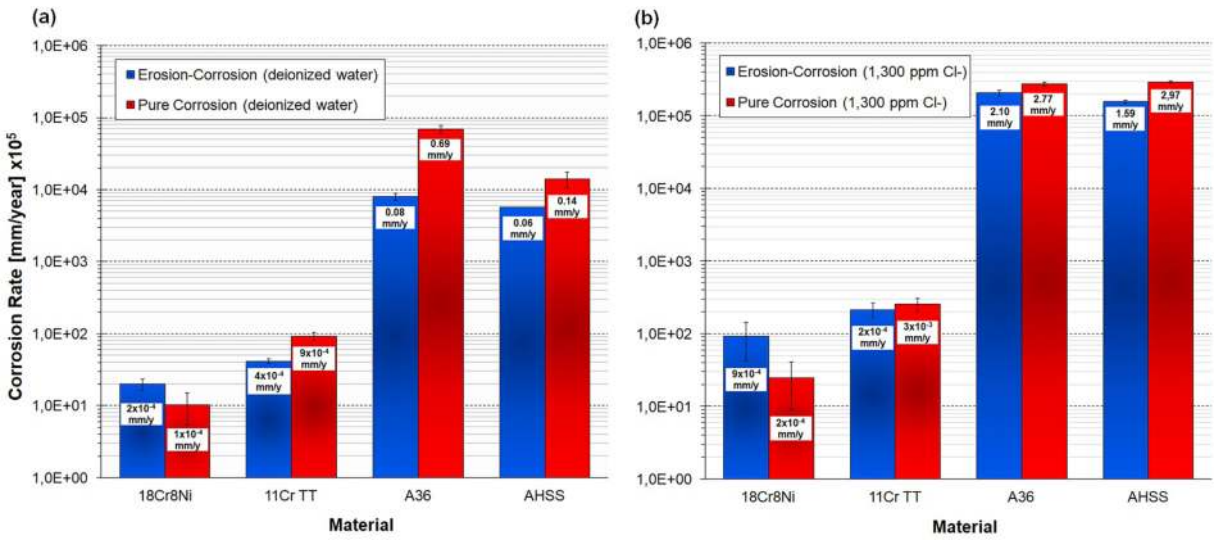

Fig. 19. Corrosion rate of the materials after 10 cycles of erosion-corrosion and pure corrosion tests on (a) deionized water and (b) 1300 ppm of chlorides media (after varnish removal and chemical cleaning of carbon steel surface).

corrosion damage was observed for the martensitic steel. This behavior can be explained by the much higher corrosion resistance of 304 steel compared to 410, although the latter, after quenching, exhibits much higher wear resistance, as confirmed by other authors [60]. In this way, the results obtained suggest that the periodic surface cleaning by the corn particles proved to be expressively beneficial for the less corrosion-resistant materials but was deleterious for the more corrosion-resistant steels. Table 4 shows the roughness, while Figs. 20 and 21 show the 3D topography of A36 and AHSS carbon steels after erosion-corrosion and pure corrosion tests.

The 18Cr8Ni and 11CrTT stainless steels were also characterized, but the surface topography remained preserved as the starting condition. Comparing to the prepared starting surface (0.202 and 0.034 μm Ra, respectively), the A36 and AHSS steels increased drastically, which in wear-corrosion conditions can represent a significant loss of performance due to surface gradients increasing [61]. The better performance of AHSS steel in erosion-corrosion is evidenced again in deionized water media when compared to A36 steel, as can be better visualized in Fig. 20. The A36 presented authentic generalized corrosion in all the surface areas, while the AHSS a more localized damage mechanism.

In the 1300 ppm chloride medium, both steels presented very similar surfaces after erosion-corrosion (Fig. 21). However, the AHSS showed a roughness peak in pure corrosion condition, revealing a more heterogeneous and damaged final surface. The chromium content (0.97%) present in the high-strength alloy significantly reduced corrosion rates in deionized water, but it had a much smaller effect in the presence of chlorides. The periodical breakdown of the rust layer and the increase of the surface roughness cause an increase in the overall corrosion rate, especially in presence of more hard particles [8]. A rougher surface favors material incrustation, which can generate operational problems for grain processing plants. The degradation of organic matter adhered to equipment can lead to contamination of the food that meets the metallic surface.

Table 4
Surface roughness of A36 and AHSS carbon steel after 10 cycles of erosion-corrosion and pure corrosion testsin deionized water and 1300 ppm of chlorides solutions.

Condition	A36	AHSS
Erosion-Corrosion (deionized water)	3.93 ± 0.83	0.75 ± 0.52
Erosion-Corrosion (1300 ppm Cl^-)	8.20 ± 1.08	8.18 ± 1.28
Pure Corrosion (deionized water)	4.33 ± 0.98	3.34 ± 2.49
Pure Corrosion (1300 ppm Cl^-)	8.08 ± 0.92	15.50 ± 2.00

3.7. Synergy between erosion and corrosion

It was considered that corrosion is the main damage process, and the effect of erosion on corrosion was investigated. Thus, the phenomenon was called erosion-enhanced corrosion. In general, the erosion enhanced corrosion synergy was not evident in the results since the corn erosive particles were not able to damage the surface or even completely remove the oxide layer from the surface to reach the metallic substrate, in the specific case of carbon steels. The absence of hardening or deformation mechanisms on the surface also corroborates this conclusion, so the higher or lower mass loss rates on erosion-corrosion were strongly influenced by the amount of rust formed on the surface. The erosion caused a reduction in the surface roughness of the steels studied, except in the case of AHSS steel (Table 3). This effect was more pronounced for A36 steel. Regarding erosion-enhanced corrosion, we can divide the materials in two groups to discuss the results: stainless steel and carbon steel.

Firstly, the two corrosive media proved to be low aggressive for the 18Cr8Ni and 11CrTT SS in the conditions tested, as can be seen in the final surfaces and mass loss rates obtained. Considering the greater corrosion resistance of the 18Cr8Ni compared to the 11CrTT SS, the corrosion damage was even lower for the 18Cr8Ni steel. On the other hand, the damage observed in pure erosion was higher for the 18Cr8NiSS, which is softer compared to the 11CrTT steel (Table 1). The erosion-enhanced corrosion rate for 18Cr8Ni was higher than its corrosion rate in the deionized water and in the medium containing chlorides. The erosion was detrimental to the corrosion rate of the 18Cr8Ni in both media, and the synergy is positive [28].

Interestingly, for the 11CrTT steel, the lower damage from pure erosion obviously impacted the lower erosion-corrosion mass loss rates when compared to pure corrosion, which is emphasized in the 1300 ppm of chlorides medium. This result, however, also suggests a beneficial effect of erosion on corrosion resistance for the 11Cr steel, mainly in the more aggressive environment containing chlorides. In this case, the synergy between erosion and corrosion is negative [28].

Regarding A36 and AHSS carbon steels, which in pure erosion tests even showed mass gain due to the formation of corrosion products, the erosion-corrosion rate was lower compared to pure corrosion in both media. A beneficial effect of erosion on the corrosion resistance of carbon steels was identified mainly in deionized water. This effect can be

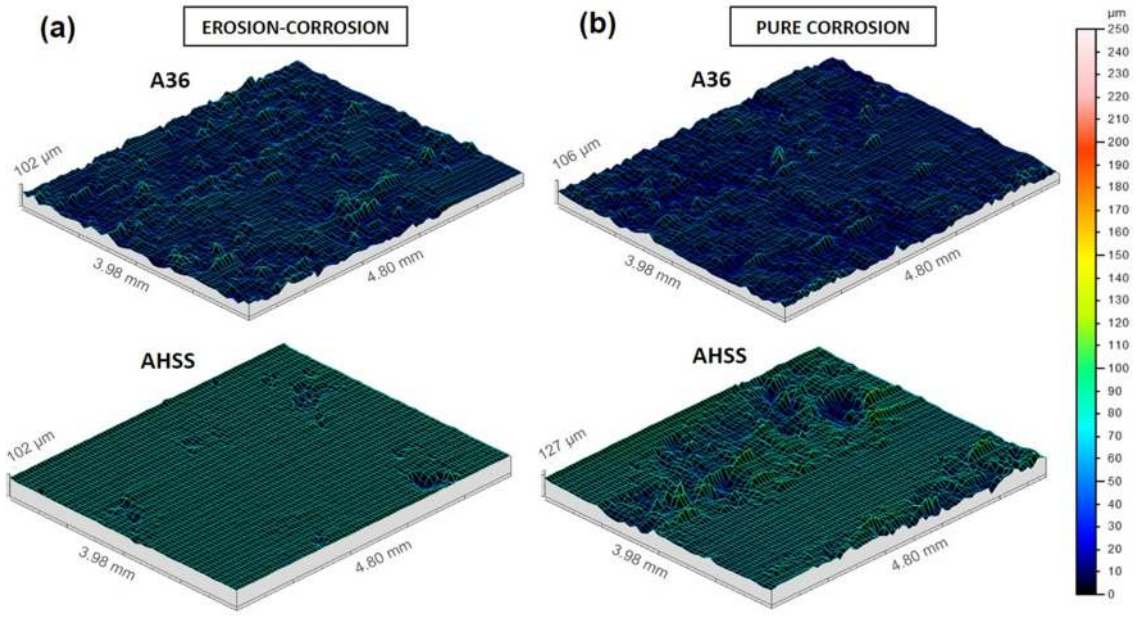

Fig. 20. 3D topography of the A36 and AHSS carbons steels after (a) erosion-corrosion and (b) pure corrosion conditions in deionized water media, respectively (surfaces after chemical cleaning).

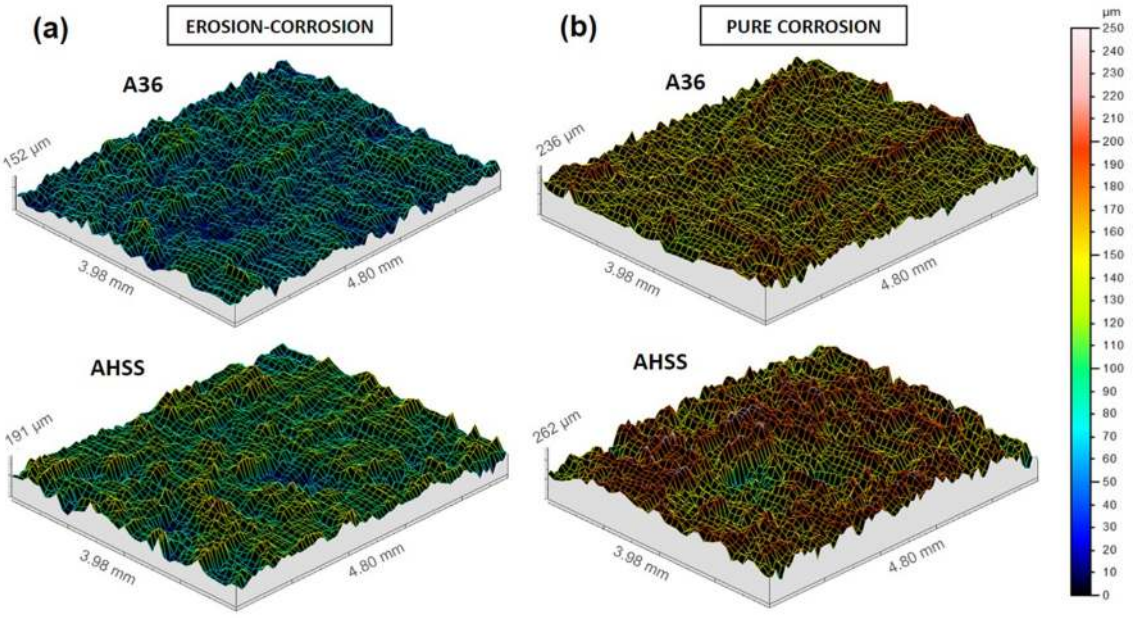

Fig. 21. 3D topography of the A36 and AHSS carbons steels after (a) erosion-corrosion and (b) pure corrosion conditions in 1300 ppm of chlorides media, respectively(surfaces after chemical cleaning).

associated with the periodic removal of non-adherent porous rusts that act as reservoirs for corrosive agents and the smoothing effect, thus attenuating corrosion damage in the erosion-corrosion test, and a negative synergy between erosion and corrosion was identified [28].

In the schematic diagram shown in Fig. 22, the different mechanisms observed in the materials due to the erosion influence on corrosion are illustrated. For the 18Cr8Ni and 11CrTT stainless steel surfaces, only the smoothing effect is pertinent (Fig. 22a), once these materials did not present corrosion products added to the macro surface to be removed. Regarding carbon steels, the corrosion was the main mechanism in the surface degradation and mass loss rates, and their effect coupled to erosion impacted directly in the rust layer dynamics. The corn particles were much more evident in these materials due to the non-adherent rust layer periodical removal action, which is illustrated in Fig. 22b for the deionized water and in Fig. 22 c for the medium containing 1300 ppm of chloride ions. As discussed previously in the surface analysis, the AHSS performed better in the less aggressive medium when compared to the A36 carbon steel. In the medium containing chlorides, evaluating the surface throughout the erosion-corrosion cycles, despite the chromium content in the chemical composition, the high-strength steel showed a very similar behavior to the conventional carbon steel.

4. Conclusions

In this study, laboratory tests were performed to study the erosion, corrosion and erosion-corrosion behavior of stainless and carbon steels,

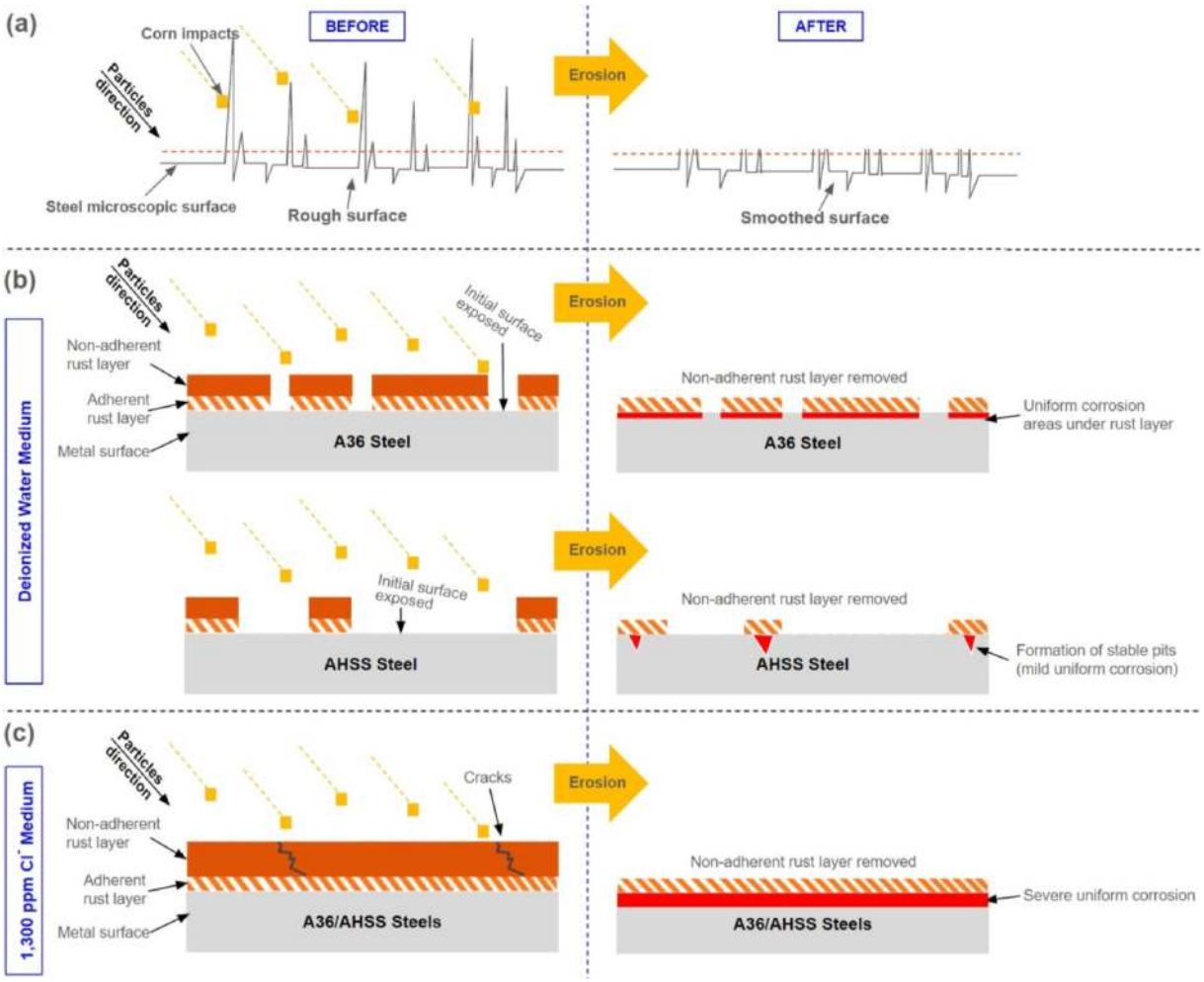

Fig. 22. Schematic diagram of erosion and corrosion mechanisms impact on the materials degradation: (a) pure erosion for all materials and erosion-corrosion for A36 and AHSS carbon steels at (b) deionized water and (c) 1300 ppm of chlorides mediums.

aimed at understanding the main mechanisms involved and establishing a more cost-effective solution to reduce equipment maintenance and environmental impacts in the agribusiness sector.

The deionized water and chlorides containing corrosive media proved to be low aggressive for the 18Cr8Ni and 11CrTT stainless steels in the conditions tested. The surfaces maintained their initial shine and mirrored appearance in addition to the very low corrosion rates observed.

Even though corn particles impact were not able to deform or cause mechanical damage to the steel surfaces, the soft erosive acts removed non-adherent corrosion products formed in the carbon steel and polishing the surfaces.

The erosive component had a evidentiated impact in the 18Cr8Ni soft surface compared to the more hard 11Cr surface, however, the corrosion damage was more significative in the 11Cr steel. The erosion-enhanced corrosion rates of 11Cr and carbon steels were lower than the pure corrosion rates. Specifically for the carbon steel this indicates that the soft particles impact was expressively beneficial due to the periodic removal of porous rust layers that function as reservoirs for corrosive agents which culminated in the corrosion damage mitigation.

The corn particle erosion associated to the corrosion component in the deionized water media leads to the AHSS corrosion pattern change from general corrosion to localized damage, significantly reducing the corrosion rates and surface degradation.

In erosion-corrosion tests, regardless of hardness, the carbon steels presented corrosion rates at least 130 times higher in the deionized water and at least 700 times higher in the chloride solution compared to the 11CrTT stainless steel.

Low-chromium stainless steel emerges as a cost-effective and environmentally friendly solution to wear and corrosion challenges in the agribusiness segment.

Declaration of competing interest

The authors declare the following financial interests/personal relationships which may be considered as potential competing interests: VANESSA DE FREITAS CUNHA LINS reports financial support was provided by Conselho Nacional de Desenvolvimento Científico e Tecnológico. Vanessa de Freitas Cunha Lins reports a relationship with Conselho Nacional de Desenvolvimento Científico e Tecnológico that includes: funding grants. If there are other authors, they declare that they have no known competing financial interests or personal relationships that could have appeared to influence the work reported in this paper.

References

[1] Cepea CNA. Agribusiness GDP. Adv Stud Cent Appl Econ 2022:19.
[2] Agroanalysis FGV. Getúlio Vargas fund, vol. 41; 2021. p. 1–5.
[3] FAO. The state of food and agriculture. Rome: Food and Agriculture Organization of the United Nations; 2016.
[4] Iannuzzi M, Frankel GS. The carbon footprint of steel corrosion 2022;6. https://doi.org/10.1038/s41529-022-00318-1. Springer US.

[5] Koch G, Varney J, Thompson N, Moghissi O, Gould M, Payer J. International measures of prevention, application, and economics of corrosion technologies study. 2016.

[6] Maher M, Iraola-Arregui I, Ben Youcef H, Rhouta B, Trabadelo V. The synergistic effect of wear-corrosion in stainless steels: a review. Mater Today Proc 2021;51:1975–90. https://doi.org/10.1016/j.matpr.2021.05.010.

[7] Labiapari WS, Pagani V, de Mello JDB, Gonçalves RJ, Cunto JC Di. Green ferritic stainless steel: a sustainable, advanced and cost-effective solution for the concrete mixer drum. Mech Mach Sci 2022;108:429–37. https://doi.org/10.1007/978-3-030-87383-7_47. MMS.

[8] Xu Y, Zhang Q, Chen H, Zhao Y, Huang Y. Experimental study on erosion-corrosion of carbon steel in flowing NaCl solution of different pH. J Mater Res Technol 2022;20:4432–51. https://doi.org/10.1016/j.jmrt.2022.09.012.

[9] Labiapari WS, Pagani V, de Mello JDB, Gonçalves RJ, Cunto JC Di, Alcântara CM de, et al. Understanding abrasion-corrosion to improve concrete mixer drum performance: A laboratory and field approach 2021;477. https://doi.org/10.1016/j.wear.2021.203830. Elsevier Ltd.

[10] Ligier K, Zemlik M, Lemecha M, Konat Ł, Napiórkowski J. Analysis of Wear Properties of Hardox Steels in Different Soil. Conditions 2022;15(21):7622.

[11] Hacısalihoğlu İ, Yıldız F, Çelik A. Tribocorrosion behavior of plasma nitrided Hardox steels in NaCl solution 2018;120. https://doi.org/10.1016/j.triboint.2018.01.023.

[12] Popovych PV, Lyashuk OL, Murovanyi IS, Dzyura VO, Shevchuk OS, Myndyuk VD. The service life evaluation of fertilizer spreaders undercarriages 2016;50.

[13] Labiapari W, Alcântara CM, Costa HL, De Mello JDB. Stainless steel as an antiwear material for the bio-fuel industry 2013;302. https://doi.org/10.1016/j.wear.2012.12.023.

[14] Walczak M, Sharifi S, Stack MM. On a multiphysics approach to modelling the erosion-enhanced corrosion of low-alloy carbon steel in chloride containing. Environments 2020;176.

[15] Xu Y, Zhang Q, Chen H, Huang Y. Understanding the interaction between erosion and corrosion of pipeline steel in acid solution of different pH. J Mater Res Technol 2023;25:6550–66.

[16] Chung RJ, Jiang J, Pang C, Yu B, Eadie R, Li DY. Erosion-corrosion behaviour of steels used in slurry pipelines. Wear 2021;477. https://doi.org/10.1016/j.wear.2021.203771.

[17] Zheng Z bin, Long J, Guo Y, Li H, Zheng K hong, Qiao Y xin. Corrosion and impact–abrasion–corrosion behaviors of quenching–tempering martensitic Fe–Cr alloy steels. J Iron Steel Res Int 2022;29:1853–63. https://doi.org/10.1007/s42243-021-00728-6.

[18] Zheng ZB, Zheng YG, Zhou X, He SY, Sun WH, Wang JQ. Determination of the critical flow velocities for erosion-corrosion of passive materials under impingement by NaCl solution containing sand 2014;88. https://doi.org/10.1016/j.corsci.2014.07.043. Elsevier Ltd.

[19] Du Y, Yang G, Chen S, Ren Y. Research on the erosion-corrosion mechanism of 304 stainless steel pipeline of mine water in falling film flow. Corrosion Sci 2022;206:110531. https://doi.org/10.1016/j.corsci.2022.110531.

[20] Sabih A, Radziszewski P, Mullany I. Investigating grinding media differences in microstructure , hardness , abrasion and fracture toughness 2017;103–104. https://doi.org/10.1016/j.mineng.2016.08.014. Elsevier Ltd.

[21] Karafyllias G, Galloway A, Humphries E. Erosion-corrosion assessment in strong acidic conditions for a white cast iron and UNS S31600 stainless steel 2021;484–485. https://doi.org/10.1016/j.wear.2021.203665. Elsevier Ltd.

[22] Camacho J, Lewis R, Dwyer-Joyce RS. Wear of a chute in a rice sorting machine. Wear 2007;263:65–73. https://doi.org/10.1016/j.wear.2006.11.052.

[23] Karafyllias G, Galloway A, Humphries E. The effect of low pH in erosion-corrosion resistance of high chromium cast irons and stainless steels 2019;420–421. https://doi.org/10.1016/j.wear.2018.11.021. Elsevier Ltd.

[24] Zeng L, Shuang S, Guo XP, Zhang GA. Erosion-corrosion of stainless steel at different locations of a 90° elbow 2016;111. https://doi.org/10.1016/j.corsci.2016.05.004. Elsevier Ltd.

[25] Yoneda S, Hayashi S, Miyakoshi Y, Kogin T, Ishikawa E, Noguchi M. Erosion-corrosion behavior of Ni-20Cr-4Fe and Ni-20Cr-4Fe-7Mo under fluidized-bed biomass boiler conditions 2022;205. https://doi.org/10.1016/j.corsci.2022.110472.

[26] Zheng ZB, Zheng YG. Erosion-enhanced corrosion of stainless steel and carbon steel measured electrochemically under liquid and slurry impingement, vol. 102. Elsevier Ltd; 2016. https://doi.org/10.1016/j.corsci.2015.10.014.

[27] Neville A, Wang C. Erosion-corrosion of engineering steels-Can it be managed by use of chemicals? Wear 2009;267:2018–26. https://doi.org/10.1016/j.wear.2009.06.041.

[28] Labiapari WS, Ardila MAN, Costa HL, de Mello JDB. Micro abrasion-corrosion of ferritic stainless steels 2017;376–377. https://doi.org/10.1016/j.wear.2017.01.083. Elsevier Ltd.

[29] López D, Falleiros NA, Tschiptschin P. Corrosion-erosion behaviour of austenitic and martensitic high nitrogen stainless steels. Wear 2007;263:347–54. https://doi.org/10.1016/j.wear.2007.01.053.

[30] Durmoo S, Richard C, Beranger G, Moutia Y. Biocorrosion of stainless steel grade 304L (SS304L) in sugar cane juice 2008;54. https://doi.org/10.1016/j.electacta.2008.06.028.

[31] Camacho J, Lewis R, Dwyer-Joyce RS. Solid particle erosion caused by rice grains 2009;267. https://doi.org/10.1016/j.wear.2008.12.034.

[32] Bahri A, Guermazi N, Elleuch K, Ürgen M. On the erosive wear of 304 L stainless steel caused by olive seed particles impact: Modeling and experiments 2016;102. https://doi.org/10.1016/j.triboint.2016.06.020. Elsevier.

[33] Naz MY, Ismail NI, Sulaiman SA, Shukrullah S. Electrochemical and Dry Sand Impact Erosion Studies on Carbon Steel 2015;5. https://doi.org/10.1038/srep16583. Nature Publishing Group.

[34] Anderson K, Karimi S, Shirazi S. Erosion testing and modeling of several non-metallic materials 2021;477. https://doi.org/10.1016/j.wear.2021.203811. Elsevier Ltd.

[35] Birkin PR, Lear R, Webster L, Powell L, Martin HL. In-situ detection of single particle impact, erosion/corrosion and surface roughening 2021;464–465. https://doi.org/10.1016/j.wear.2020.203527. Elsevier Ltd.

[36] Chen Z, Wassgren C, Ambrose RPK. A review of Grain Kernel Damage: Mechanisms, Modeling, and Testing Procedures 2020;63:455–75.

[37] Han Y, Zhao D, Chu Y, Zhen J, Li G, Zhao H, et al. Breakage behaviour of single rice particles under compression and impact. Adv Powder Technol 2021;32:4635–50. https://doi.org/10.1016/j.apt.2021.10.017.

[38] ASTM. ASTM B117: Standard Practice for Operating Salt Spray (Fog) Apparatus 2003;1. https://doi.org/10.1177/089033449801400218.

[39] ASTM. ASTM D1193-99: Standard Specification for Reagent Water 2001;51.

[40] ASTM. ASTM G1-03: Standard Practice for Preparing, Cleaning, and Evaluating Corrosion Test Specimens 2017;i. https://doi.org/10.1520/G0001-03R17E01.2.

[41] Yu Y, Shironita S, Souma K, Umeda M. Effect of chromium content on the corrosion resistance of ferritic stainless steels in sulfuric acid solution. Elsevier Ltd; 2018. https://doi.org/10.1016/j.heliyon.2018.e00958.

[42] Faria GL de, Godefroid LB, Nunes IP, Lacerda JC de. Effect of martensite volume fraction on the mechanical behavior of an UNS S41003 dual-phase stainless steel. Mater Sci Eng, A 2020;797. https://doi.org/10.1016/j.msea.2020.140208.

[43] Ojala N, Valtonen K, Heino V, Kallio M, Aaltonen J, Siitonen P, et al. Effects of composition and microstructure on the abrasive wear performance of quenched wear resistant steels. Wear 2014;317:225–32. https://doi.org/10.1016/j.wear.2014.06.003.

[44] ASTM. ASTM G 171 - Standard Test Method for Scratch Hardness of Materials Using a Diamond Stylus 1 2009;3. https://doi.org/10.1520/G0171-03R17.2.

[45] Zhang Y, Yin X, Wang J, Yan F. Influence of microstructure evolution on tribocorrosion of 304SS in artificial seawater. Corrosion Sci 2014;88:423–33. https://doi.org/10.1016/j.corsci.2014.07.062.

[46] He Y, Yoo KB, Ma H, Shin K. Study of the austenitic stainless steel with gradient structured surface fabricated via shot peening, vol. 215. Elsevier B.V.; 2018. https://doi.org/10.1016/j.matlet.2017.12.021.

[47] Lv J, Guo W, Liang T. The effect of pre-deformation on corrosion resistance of the passive film formed on 2205 duplex stainless steel 2016;686. https://doi.org/10.1016/j.jallcom.2016.06.003. Elsevier Ltd.

[48] Soares FM de S, Barbosa DM, Corado HPR, Santana AI de C, Elias CN. Surface morphology, roughness, and corrosion resistance of dental implants produced by additive manufacturing. J Mater Res Technol 2022;21:3844–55. https://doi.org/10.1016/j.jmrt.2022.10.114.

[49] Ardila MAN, Labiapari WS, Costa HL, de Mello JDB. Influence of stainless steel specimen topography on micro-abrasion and micro-abrasion-corrosion. Wear 2019;426–427:1482–95. https://doi.org/10.1016/j.wear.2019.01.011.

[50] Niskanen I, Lauri J, Räty J, Heikkilä R, Liimatainen H, Hashimoto T, et al. Monitoring drying process of varnish by immersion solid matching method. Prog Org Coatings 2019;136:105299. https://doi.org/10.1016/j.porgcoat.2019.105299.

[51] García KE, Barrero CA, Morales AL, Greneche JM. Lost iron and iron converted into rust in steels submitted to dry-wet corrosion process. Corrosion Sci 2008;50:763–72. https://doi.org/10.1016/j.corsci.2007.09.003.

[52] Pérez FR, Barrero CA, García KE. Factors affecting the amount of corroded iron converted into adherent rust in steels submitted to immersion tests. Corrosion Sci 2010;52:2582–91. https://doi.org/10.1016/j.corsci.2010.04.005.

[53] Sun B, Zuo X, Cheng X, Li X. The role of chromium content in the long-term atmospheric corrosion process 2020;4. https://doi.org/10.1038/s41529-020-00142-5. Springer US.

[54] Tamura H. The role of rusts in corrosion and corrosion protection of iron and steel. Corrosion Sci 2008;50:1872–83. https://doi.org/10.1016/j.corsci.2008.03.008.

[55] García KE, Morales AL, Barrero CA, Greneche JM. New contributions to the understanding of rust layer formation in steels exposed to a total immersion test 2006;48:2813–30. https://doi.org/10.1016/j.corsci.2005.09.002.

[56] Hao X, Zhao X, Chen H, Huang B, Ma J, Wang C, et al. Comparative study on corrosion behaviors of ferrite-pearlite steel with dual-phase steel in the simulated bottom plate environment of cargo oil tanks. J Mater Res Technol 2021;12:399–411. https://doi.org/10.1016/j.jmrt.2021.02.095.

[57] Kayali Y, Anaturk B. Investigation of electrochemical corrosion behavior in a 3.5wt.% NaCl solution of boronized dual-phase steel. Mater Des 2013;46:776–83. https://doi.org/10.1016/j.matdes.2012.11.040.

[58] Giourntas L, Hodgkiess T, Galloway AM. Comparative study of erosion – corrosion performance on a range of stainless steels 2015;333. https://doi.org/10.1016/j.wear.2014.12.052. Elsevier.

[59] Andrews N, Giourntas L, Galloway AM, Pearson A. Erosion-corrosion behaviour of zirconia, WC-6Co, WC-6Ni and UNS S31600. Int J Refract Met Hard Mater 2015;48:229–37. https://doi.org/10.1016/j.ijrmhm.2014.09.001.

[60] Giourntas L, Brownlie F, Hodgkiess T, Galloway AM. Influence of metallic matrix on erosion-corrosion behaviour of high chromium cast irons under slurry impingement conditions, vol. 477. Elsevier B.V.; 2021. https://doi.org/10.1016/j.wear.2021.203834.

[61] Sajjad U, Abbas A, Sadeghianjahromi A, Abbas N, Liaw JS, Wang CC. Enhancing corrosion resistance of Al 5050 alloy based on surface roughness and its fabrication methods; an experimental investigation. J Mater Res Technol 2021;11:1859–67. https://doi.org/10.1016/j.jmrt.2021.01.096.